The Science and Technology Journal of AWE

Discovery 20

May 2010

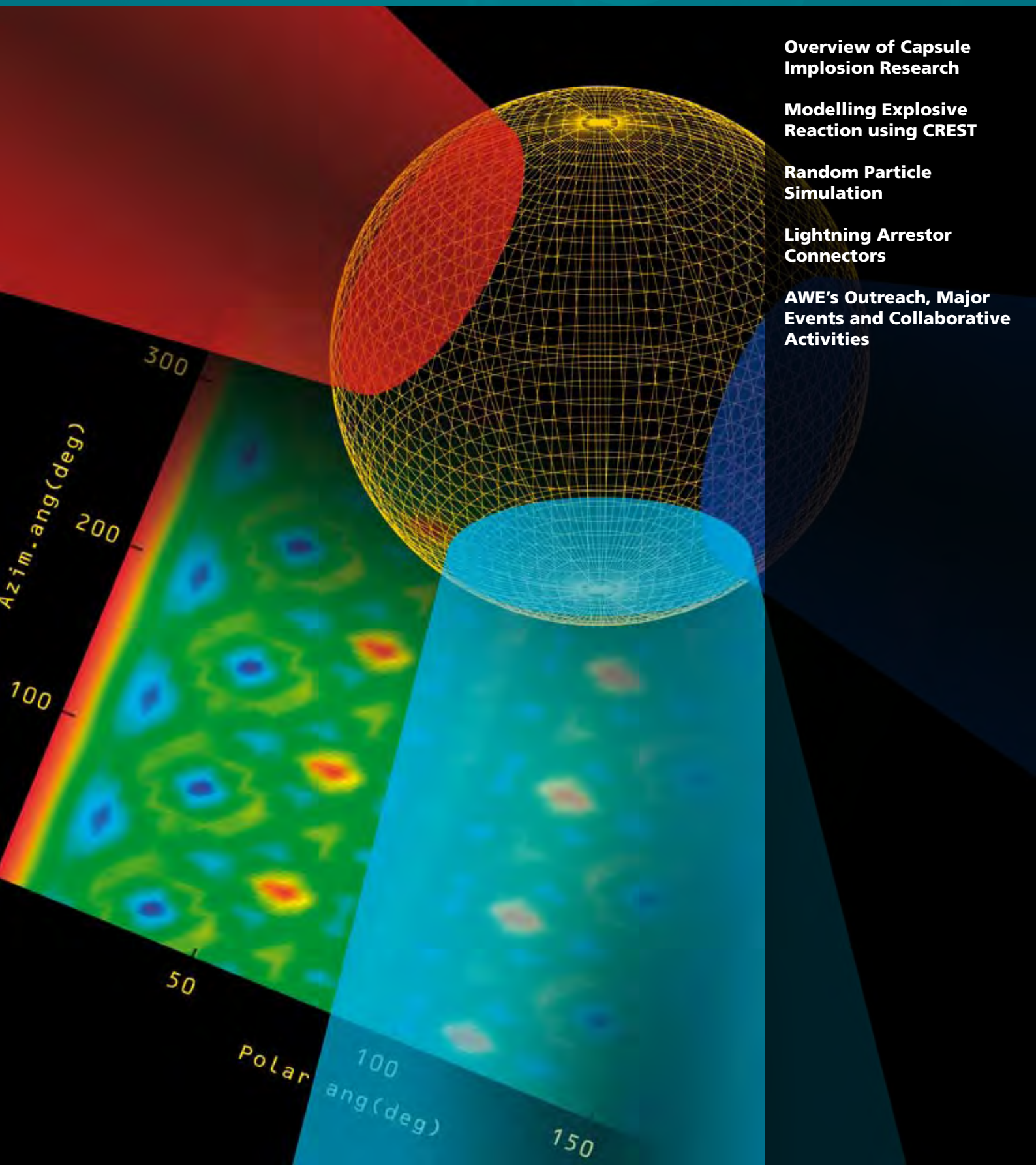

Discovery

Contents

cover image
Visualisation of laser and target configuration for capsule implosion experiments performed at the Omega laser facility

20

It is my pleasure to introduce the 20th edition of Discovery, and my first as editor. The first edition of Discovery was published a decade ago, in March 2000, with the aim of showcasing the diversity and quality of Science, Engineering and Technology (SET) undertaken at AWE.

Dr David Glue, the previous editor, should be congratulated for the excellent contribution he made, through Discovery, in recognising Science, Engineering and Technology at AWE and evolving Discovery into its present format. I am looking forward to publicising the tremendous capabilities of AWE's SET community in pursuit of our strategic defence mission for the UK Government.

The core of AWE work is multi-disciplinary Science, Engineering and Technology partnerships. Such partnerships, whether between internal teams at AWE or through external interactions with academia or industry, are fundamental to developing and applying solutions to the complex problems we face today. Many of the challenges, as exemplified in this edition, cover unusual environments of high temperature, pressure, voltage and very short timescales. It is through the combination of theoretical modelling and high fidelity experimentation that we satisfy ourselves in our understanding of the phenomena present in nuclear weapon performance in an era without further nuclear tests. As time marches on from the nuclear test database, the future challenges will place a greater emphasis on our SET capability and our external interactions will play a key role.

The Outreach article in this addition highlights how AWE is building partnerships with UK academia to strengthen and develop both our own internal and national capabilities. As AWE continues to provide high quality SET for strategic defence and national security, I hope Discovery can continue to communicate some of the important work we do. I hope you continue to enjoy this and future editions of Discovery.

Dr Graeme Nicholson
Director Science & Technology

Overview of Capsule Implosion Research

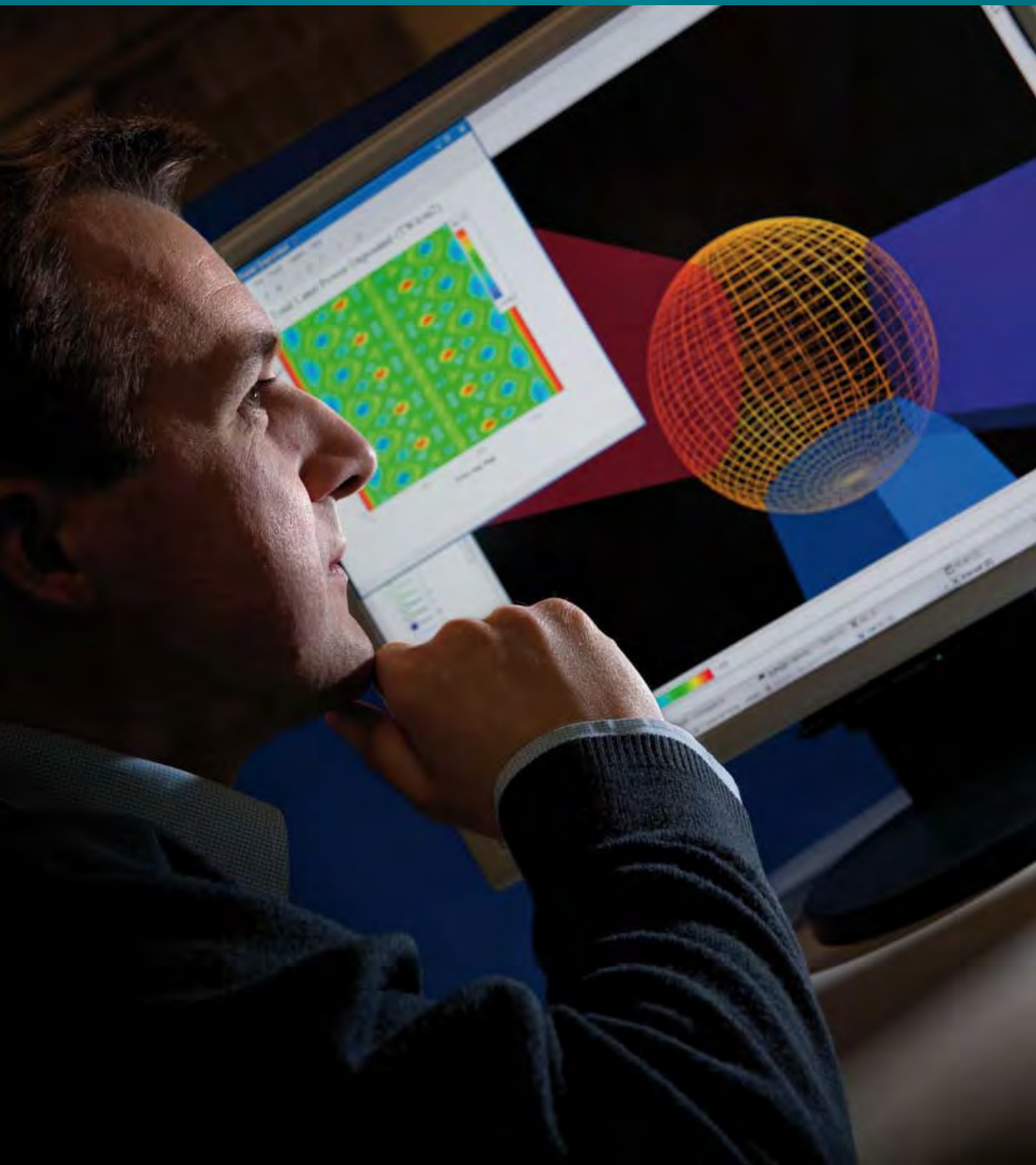

Capsule implosions are used to study a variety of physics phenomena relevant to inertial confinement fusion (ICF)[1] and basic physics research. Applications include the study of implosion hydrodynamics, for both simple and complex implosions,[2] validation of hydrodynamic mix models and thermonuclear fusion. Implosion experiments provide an excellent way to routinely generate hot dense plasma conditions.

Much of AWE's research in this area is carried out through collaboration with Los Alamos National Laboratory (LANL) and Lawrence Livermore National Laboratory (LLNL) in the US. Experiments are performed using the 60-beam OMEGA laser facility at the Laboratory for Laser Energetics (LLE), University of Rochester.[3] This provides the large drive energies necessary to produce sizeable fusion yields and the large number of laser beams ensures highly symmetric implosions. Some early implosion experiments were successfully performed on AWE's two-beam HELEN system in 1981 using simple 'exploding pusher' targets, which are more robust to asymmetry. These were recalculated in 2007 using modern code tools and the results were found to agree well with the observed data.[4]

Currently work is focussed toward activities on the US National Ignition Facility (NIF).[5] Designed to achieve thermonuclear ignition of ICF capsules, NIF will allow implosions to be performed at much higher drive energies than is presently possible and offers the prospect of directly studying igniting plasmas.

In readiness for experiments throughout the next decade, work is underway to resolve important issues and develop diagnostic techniques. AWE is collaborating in three separate campaigns designed to study fuel mixtures, the effects of fuel dopants and the development of a burn history diagnostic.

Burn History Diagnostic

A requirement for understanding NIF implosions is the measurement of accurate capsule implosion times and highly time-resolved thermonuclear reaction histories (burn rate versus time). Such measurements can be used to identify failure modes of ignition capsules,[6] distinguishing shock timing errors from irradiation asymmetries and other factors. Reaction history measurements are potentially invaluable for constraining energy modelling and hydrodynamic mix in any capsule implosion.

A reaction history diagnostic is being designed for NIF based on detection of the 16.7 MeV gamma rays occasionally produced in the deuterium-tritium (DT) fusion reaction. Although this mode has an unfavourable branching ratio of ~ 5×10^{-5} compared to the production of 14 MeV neutrons, high implosion reaction rates are sufficient to overcome this and make the technique viable. Gamma ray diagnostics remove time-of-flight issues and can thus provide high bandwidth, high reaction rate measurements which complement neutron-based methods.

The NIF diagnostic, which is being developed and tested by a LANL-AWE-LLNL team,[7] will use Gas Cherenkov detectors (GCDs) to measure the arrival of 16.7 MeV gamma rays. In these instruments fusion gammas undergo Compton scattering and pair production interactions in a low Z converter, e.g. beryllium, to produce high

"In readiness for experiments throughout the next decade, work is underway to resolve important issues and develop diagnostic techniques."

FIGURE 1

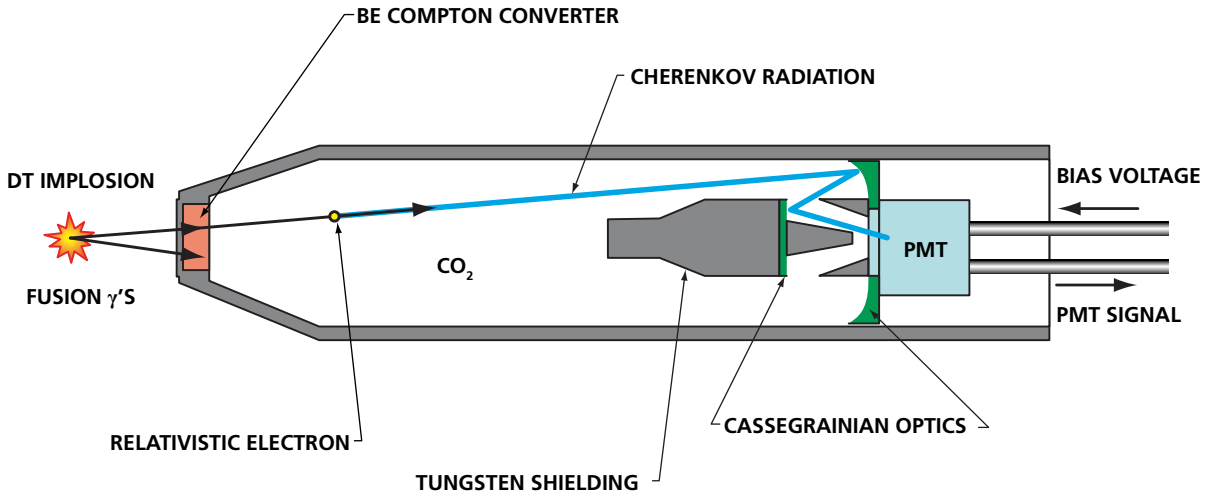

Gas Cherenkov burn history diagnostic.

energy electrons. The electrons propagate through a chamber of pressurised gas such as CO_2 or SF_6, giving rise to Cherenkov radiation. This radiation can be detected using either streak cameras (for high bandwidth measurements) or fast photomultiplier microchannel plate detectors (MCPs). A schematic of the GCD currently in use at OMEGA is shown in Figure 1.

A major challenge in diagnosing the burn history of NIF ignition capsules is achieving an optimal compromise between bandwidth and dynamic range. Calculations of ignition failure modes show that the reaction history contains critical information over nearly 12 orders of magnitude, with a first shock arrival at 10^8 neutrons per ns up to the expected ignition peak value at 10^{20} neutrons per ns.

"A major challenge in diagnosing the burn history of NIF ignition capsules is achieving an optimal compromise between bandwidth and dynamic range."

A multiplexed detector system has been envisaged that interlaces a streak camera and MCP recordings from a single GCD instrument to achieve coverage over an extended range. Such a concept has been successfully demonstrated by the GCD team using a LINAC electron beam source at Idaho State University.[8] This technology has not yet been applied to laser experiments.

A simpler system, consisting of a GCD connected to a photo-multiplier tube (PMT), has been used as a diagnostic on a variety of OMEGA implosion experiments. These have included cryogenic capsule experiments as part of the LLE direct drive ignition research programme.

A good illustration of GCD capabilities is provided by the Double Pulse experiments. In this experiment two temporally

FIGURE 2

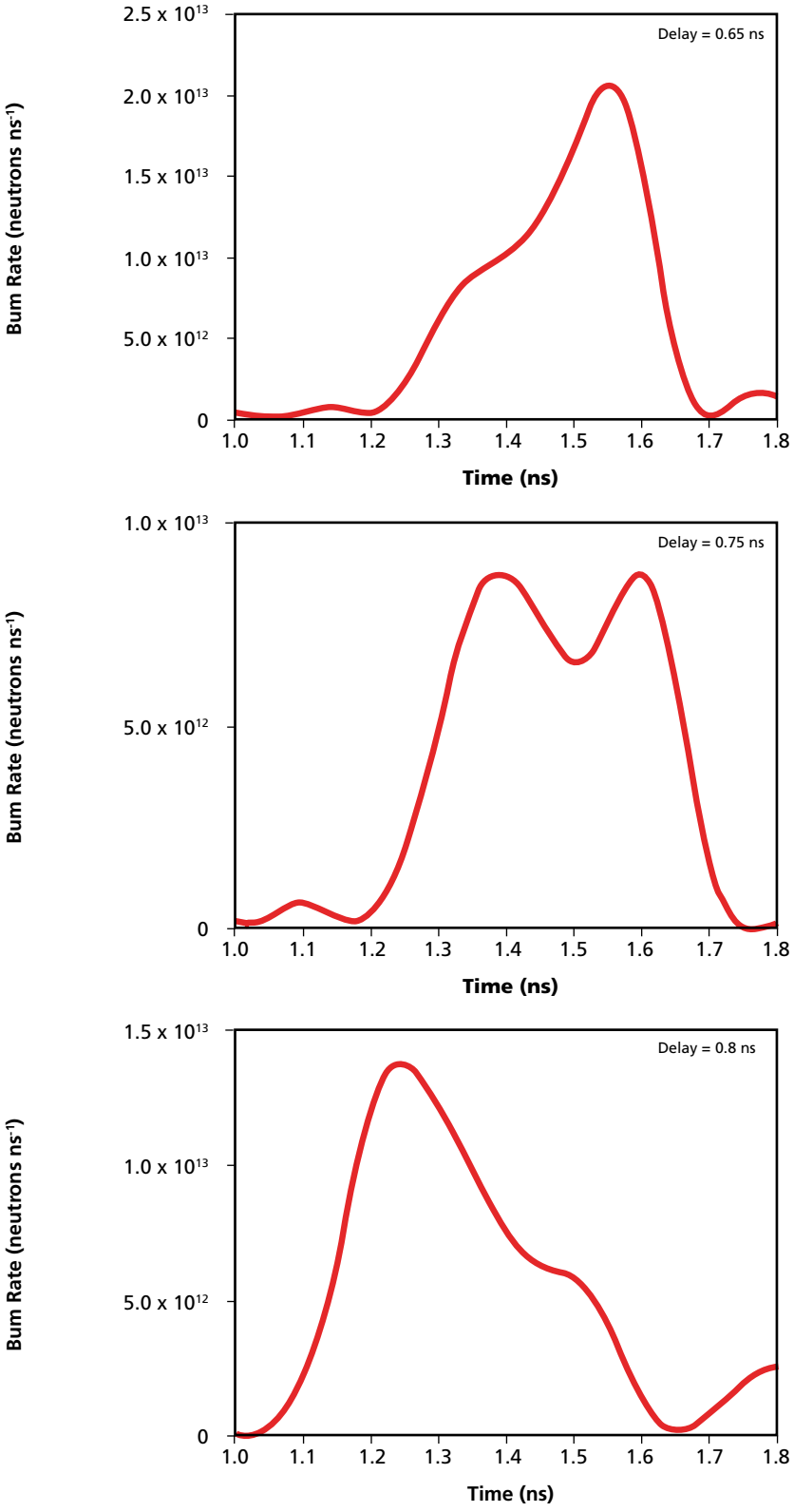

GCD data from the double pulse experiments clearly show the evolution of the fusion reaction history as the delay between the drive pulses is varied.[9]

separated laser pulses are used to obtain a double peaked fusion reaction history from a DT filled glass capsule.[9] These experiments provide a test bed for ICF mix models. As the delay between the two drive pulses was varied the GCD was able to capture the evolution of the burn history. This is shown in Figure 2.

Experiments on Fuel Mixtures

A standard technique in ICF implosion research is the use of DHe^3 fuels to improve diagnosis of compressed core conditions. In addition to DD neutrons, these fuels also generate 14.7 MeV protons via the DHe^3 fusion reaction. These readily escape from the capsule and can be detected by a range of charged particle diagnostics.

Measurements of the proton spectra can be used to provide additional constraints on the areal density and ion temperature of the fuel.

Recent experiments have suggested that CH capsules containing He^3 do not behave as expected.[10] Using DHe^3 fuels of varying composition it was found that both neutron and proton yields are anomalously degraded in fuel mixtures, relative to the pure deuterium case. In an attempt to understand these results and quantify the impact on thin-shell glass capsules AWE has been involved in two separate experiments, with LANL.

The first experiment compared capsules fuelled with D_2 against some containing an 80:20 (atomic) mixture of DHe^3. The fuel pressures were chosen to satisfy hydrodynamic equivalence, as defined by Rygg et al.[10] in order to maintain consistent implosion dynamics. In some cases a small quantity of Kr was added to the fuel to facilitate spectroscopic diagnosis. A range of nuclear particle diagnostics and x-ray imaging was used in order to look for variations in both yield and fuel compression.

Although the measurements appear to suggest an anomalous effect, a more detailed assessment has shown the data to be inconclusive. Calculations performed using the NYM hydrocode[11] show that the condition of hydrodynamic equivalence is in general not well satisfied, particularly when the capsules contain Kr. This is largely a result of non-equilibrium effects. Thus conclusions drawn from x-ray images of Kr-doped capsules may not be valid. In the cases where the capsules can be considered equivalent, the anomalous effect on neutron yield is not large enough to be statistically significant. Further shots are being performed to improve the data and increase statistical confidence.

FIGURE 3

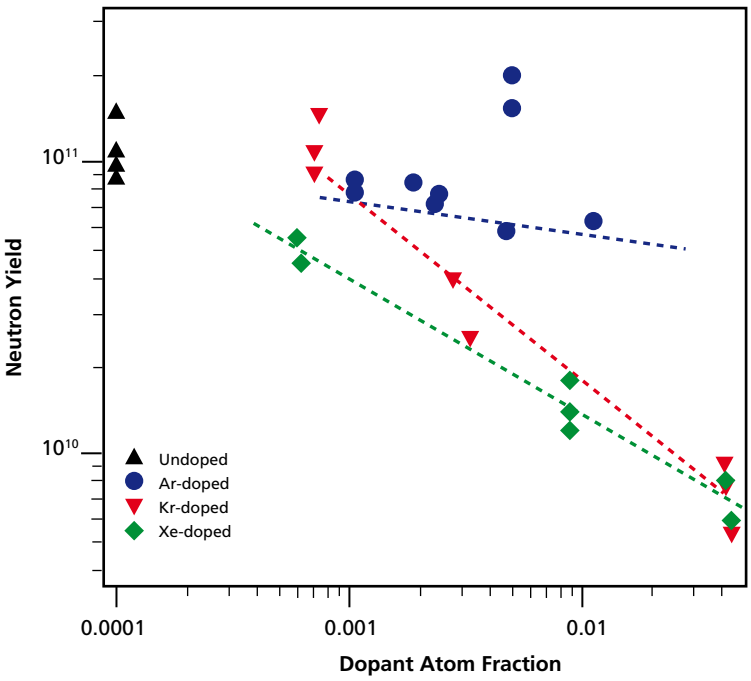

Measured neutron yields as a function of dopant atom fraction. Yields from undoped capsules are plotted at 10^{-4} for reference.

"Reaction history measurements are potentially invaluable for constraining energy modelling and hydrodynamic mix in any capsule implosion."

In the second experiment, capsules were filled using He^3 and a fixed quantity of DT fuel.[12] The use of DT rather than D_2 allowed the GCD burn history diagnostic to be fielded. The analysis of these shots has revealed some very useful insights.

Calculations predict that the amount of hydrodynamic mixing should decrease as He^3 is added. However, observations show that it is necessary to artificially increase the mix with increasing He^3 in order to match the experimental yield trend. This suggests that 1D mixing is not the dominant yield degradation mechanism in these experiments.

The GCD data were analysed by decomposing the measured signals into two Gaussian components, representing the shock and compression phases. The shock phase was found to agree well with calculation and varied little with He^3. In contrast, the measured compression phase gave a lower burn rate and duration than calculated, and was found to decrease with He^3 faster than predicted by calculation.

The results from both these experiments are consistent with the capsule compression being modified by the presence of He^3 in a manner that is not predicted by calculation. The effect may be less apparent in these thin-shell glass capsules than in the thicker CH capsules previously studied,[10] since these capsules behave more like exploding pushers with performance less dominated by the compression phase. New experiments are being designed to further explore these effects.

Doped Capsule Experiments

The use of spectroscopic dopants as a diagnostic in ICF implosions is an established technique[13] used to provide information on fuel conditions and to aid the study of hydrodynamic mixing. By using small amounts of low Z dopant,

FIGURE 4

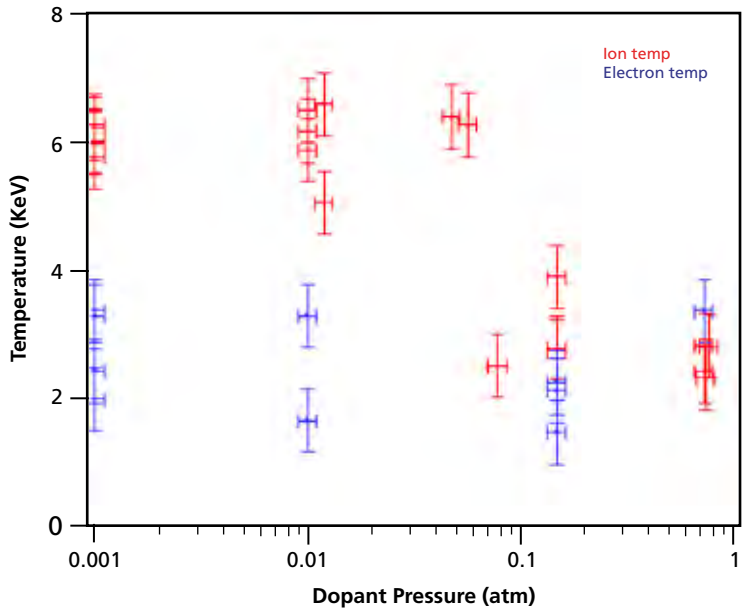

Experimentally determined ion and electron temperatures for the capsule fuel reveal the transition to equilibrium as the amount of Kr dopant is increased.

emission spectra can be obtained without significantly perturbing capsule performance. However as ignition is approached on NIF, increased fuel temperatures will necessitate the use of higher Z dopants. These have much greater potential to modify implosion behaviour.

A series of directly driven implosion experiments has been performed at the OMEGA laser to examine the effects of fuel dopant on capsule performance as both dopant concentration and atomic number are varied. These experiments are intended to guide the modeling of capsule fuel dopants ahead of future application on NIF.

The targets consisted of thin shell glass capsules filled with 10 atm of DHe^3 fuel (80:20 by atom) plus an additional quantity (up to 0.7 atm) of higher Z dopant gas. Particle yields and energy spectra were measured using standard techniques.[14] The higher Z dopant gas, e.g. Ar, Kr or Xe, is used to modify the plasma conditions. At the highest dopant pressures the dopant comprised up to 75% of the fill mass, significantly perturbing the implosion. A small quantity of Kr was maintained in all doped capsules to facilitate spectroscopic diagnosis of electron temperature.

Neutron and proton yield data are shown in Figure 3. At low dopant levels ($\leq 10^{-2}$ atm) capsule performance is little changed from the undoped case. At higher levels the yield falls off rapidly with increasing dopant pressure. The yield trends appear to be consistent with dopant Z.

1D NYM simulations provide a qualitative understanding of capsule dynamics. Ion and electron temperatures become separated by the passage of the initial shock and then relax toward equilibrium as the fuel is compressed. Yield production is dominated by the compression phase. As dopant concentration is increased the inward shock becomes weakened by radiation loss and the compression phase becomes even more dominant. At high dopant levels temperature separation is severely reduced, so that capsule yield is produced under equilibrium conditions. This transition to equilibrium is observed experimentally, as shown by Figure 4.

Comparison of simulated and measured neutron yields shows reasonable agreement. The ratio of the experimental yield over calculated clean (YoC) ranges from approximately 10 to 35%. This is consistent with results achieved in other high convergence capsule implosions,[15] demonstrating a first order understanding of capsule behaviour. Agreement becomes considerably less good at high dopant levels. This discrepancy cannot be accounted for by either hydrodynamic mix or experimental uncertainty. This seems suggestive of errors in the dopant modeling. Analysis effort is presently focused on a re-examination of non-local thermodynamic equilibrium (non-LTE) opacity models.

"At high dopant levels temperature separation is severely reduced, so that capsule yield is produced under equilibrium conditions. This transition to equilibrium is observed experimentally."

Summary

The current implosion programme is focused toward future activities on the US National Ignition Facility, which will provide the capability to perform implosions at much higher drive energies than is presently possible and offers the prospect of directly studying igniting plasmas. In readiness for experiments throughout the next decade, work is underway at the OMEGA facility, in collaboration with LANL and LLNL, to resolve important issues and develop key diagnostic techniques.

Acknowledgements

AWE's Capsule Implosion Research programme is performed by a dedicated team of which the author is just one member. He would like to highlight the role of the other members of the team. In particular; Dr Colin Horsfield, Dr David Drew and Michael Rubery.

AWE's involvement in the experiments described here is only possible through the invitation of LANL. We gratefully acknowledge this collaboration and express our thanks to the many US colleagues upon which this work relies. In particular; H W Herrmann, J M Mack, G A Kyrala, D C Wilson, S C Evans, P Sanchez, T J Sedillo, S E Caldwell, C S Young, J Langenbrunner, J F Benage, J H Cooley and F J Wysocki.

References

1 J Lindl, Phys. Plasmas 2, 3933 (1995)
2 W S Varnum et al., Phys. Rev. Lett. 84, 5153 (2000)
3 J Soures et al., Phys. Plasmas 3, 2108 (1996)
4 B R Thomas, J. Phys. Conf. Series 112, 012006 (2008)
5 E Moses, Fusion Sci. Tech. 44, 11 (2003)
6 D C Wilson, Proc 35th Anomalous Absorption Conf, Puerto Rico (2005)
7 J M Mack et al., Nucl. Instrum. Methods Phys. Res. A 513, 566 (2003)
8 J M Mack et al., Rev. Sci. Instr. 77 10E728 (2006)
9 H Herrmann, private communication
10 J R Rygg et al., Phys. Plasmas 13, 052702 (2006)
11 P D Roberts, S J Rose, P C Thompson and R J Wright, J. Phys. D 13, 1957 (1980)
12 H W Herrmann et al., Phys Plasmas 16, 056312 (2009)
13 B Hammel et al., Phys. Rev. Lett. 70, 1263 (1993)
14 G A Kyrala et al., High Energy Density Physics 3, 163 (2007)
15 P Amendt, R E Turner and O L Landen, Phys. Rev. Lett. 89, 165001 (2002)

AUTHOR PROFILE

Warren J Garbett can be contacted on e-mail: Warren.J.Garbett@awe.co.uk

Warren Garbett • Warren read for his MA and MSci in Natural Sciences at St John's College, Cambridge, where he specialised in Physics and graduated with 1st class honours. He subsequently obtained an MSc in Geophysics at Imperial College, London. He joined the Plasma Physics Department of AWE in 2000 as a member of the modelling team, applying theory and computer code simulations to the design and analysis of laser-driven experiments. He has since been involved in a number of projects, including the technical case for the ORION laser. Warren now leads the research programmes on implosion physics and thermonuclear fusion. He is recognised as one of the company authorities on inertial confinement fusion (ICF).

Modelling Explosive Reaction using CREST

Explosives used within AWE are amazing substances which are expected to lie quietly on a shelf for years and then deliver a large amount of energy within a few millionths of a second. The risk of accidental initiation of such materials is tiny, but AWE is required to demonstrate their stability under a wide variety of conditions. One of the ways to do this is through theoretically modelling the explosives' response to a range of what are euphemistically called "insults".

There are a wide range of insults which can be applied to an explosive charge, unintentionally releasing some or all of the explosive's energy. These insults can be as diverse as a fuel fire, dropping the charge onto a gritty surface or accidentally firing a projectile into it. The response of the explosive can be very different depending on the exact circumstances of the insult, so predicting the response is difficult.

Military explosives are often formulated to minimise their sensitivity to lower energy insults. Plastic bonded explosives (PBXs) have explosive crystals coated with a plastic binder that minimises the friction between crystals subjected to compressive or shearing stresses. To cope with higher energy insults Insensitive High Explosives (IHEs) utilise insensitive explosive molecules such as triaminotrinitrobenzene (TATB) and are often PBXs as well.

Any explosive that has pores, crystalline defects or indeed any sort of density discontinuities in its structure is potentially vulnerable to being initiated by a shock wave. This article is concerned with shock wave insults and a new method of modelling them. Box 1 discusses the phenomena in the shock wave growth to detonation and an experimental method of measuring it using gauges embedded in the explosive.

In order to simulate explosive behaviour the traditional basis of most models over the past 50 years has been to assume that the reaction rate is a function of a parameter (usually pressure) in the flow behind the shock. This produces a highly coupled relationship between the parameter and the reaction rate e.g. the local pressure produces a reaction rate that in turn increases the local pressure.

The approach discussed in this article is based on experimental in-material velocity gauge results. Neither reaction nor reaction rate are directly measured by the gauges but there are markers in the gauge traces that indicate the growth of reaction. One such marker is the time between the shock and the peak particle velocity, indicated as Δt in Figure 1, which reduces with increasing gauge depth and becomes zero at a little before the point of detonation.

FIGURE 1

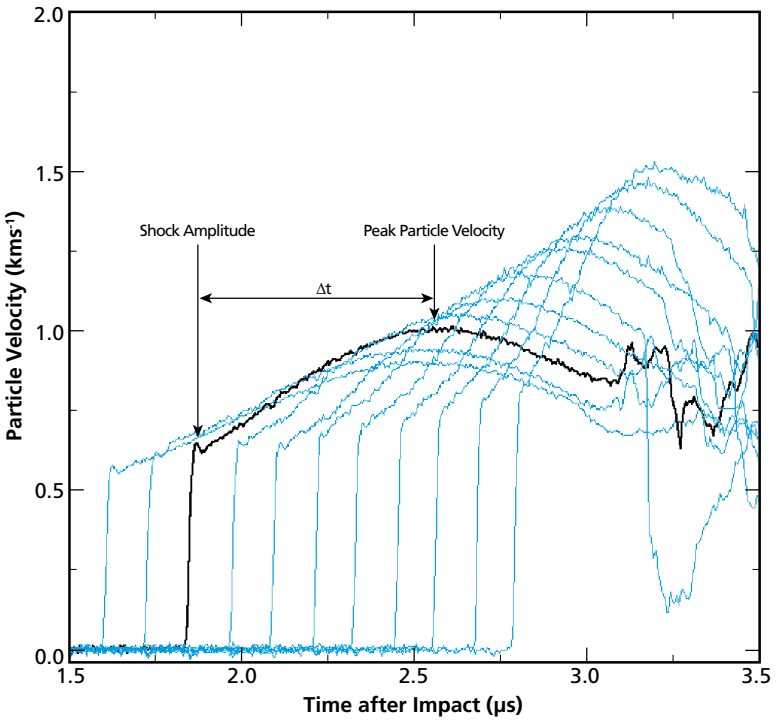

Reaction markers in a particle velocity trace for a particular gauge element. Surrounding gauge element traces are shown in blue.

Figure 2 shows data from the explosive EDC37 subjected to initial shock conditions ranging from 2.8 to 10.8 GPa. There is a monotonic relationship between Δt and the local shock strength that is followed regardless of the initial impact pressure to which the explosive was subjected. Hence the events at a particular gauge element are largely insulated from events at other gauge locations.

This insulation from previous events is so marked that where double shocks are generated in the explosive and after the second shock overtakes the first to form a single shock, the Δt relationship follows that of the single sustained pulse.

It was also found that the particle velocity histories at the same shock strength have shapes that are either identical for IHEs or can be scaled using a simple scaling factor for more sensitive explosives.

Figure 3 shows particle velocity gauge results for two shock experiments on the IHE PBX9502. The PBX9502 was subjected to two different initial pressures and the shock waves in the explosives evolved to the same shock strength at different depths. The traces at this common shock strength are almost identical.

FIGURE 2

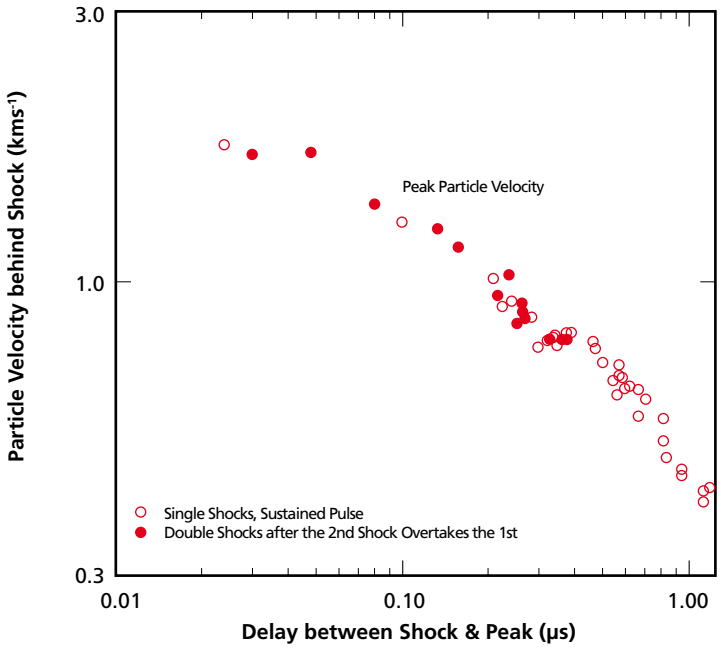

Data from experimentation on EDC37 subjected to initial shock conditions ranging from 2.76 - 10.8 GPa.

Since Δt is related to reaction, the Δt plot and the existence of scaling suggest that reaction is only a function of the local shock strength and time. This reaction changes the flow parameters, such as increasing the pressure and particle velocity behind the shock front.

"The Δt plot and the existence of scaling suggest that reaction is only a function of the local shock strength and time."

The increase in flow parameters does not immediately increase the reaction. The change in reaction is achieved by the compression waves, generated by the enhanced pressure, being propagated through the flow to interact with the shock front. This increases the amplitude of the shock, which only then increases the reaction.

The description of reaction is incorporated into a model called CREST (Computational Reaction Evolution dependent on entropy (S) and Time). The basis of CREST is that the reaction rate history at a given point in the explosive is determined by the local shock strength. This provides a more weakly coupled description of reaction than that used in all other reaction rate models. The reaction rate in CREST is based on the entropy of the unreacted

FIGURE 3

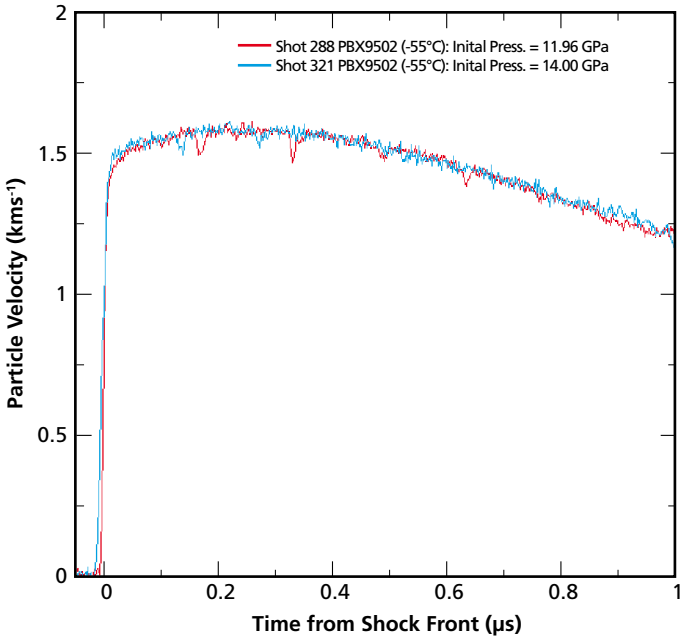

Particle velocity traces at the same shock strength, but at different depths into the explosive, for PBX9502.

explosive. Box 2 gives a brief outline of how entropy is used to generate the CREST reaction rate. The remainder of this article demonstrates the use of CREST in modelling explosives.

Shock Initiation

Parameters for the CREST model have been developed for both the insensitive explosive PBX9502 and the HMX-based explosive EDC37. The parameter values were obtained by fitting CREST to in-material gauge results for each of the explosives. Figure 4 and the Pop Plot in Box 3 show results from the experiments, which were used to calibrate the reaction-rate coefficients for PBX9502. A single set of parameter values provides a good fit over a wide range of initial shock conditions.

CREST can predict a variety of shock initiation phenomena without changing any of the parameters that determine the reaction rate. In addressing the same phenomena other reaction models require changes in the parameter values or even additional criteria. Three examples are considered which compare the CREST approach with standard methods of shock initiation modelling.

The first example is a double shock experiment in EDC37. The first shock was 2.87 GPa and the second 6.20 GPa, with a 0.65 μs delay between the shocks. Figure 5 shows the results of this experiment and the CREST calculated response.

CREST provides a reasonably good fit to the data by using an entropy based reaction rate. In contrast, pressure based reaction models over-predict the generation of reaction by the second shock and require a "desensitization" criterion, in addition to the reaction model, to

FIGURE 4

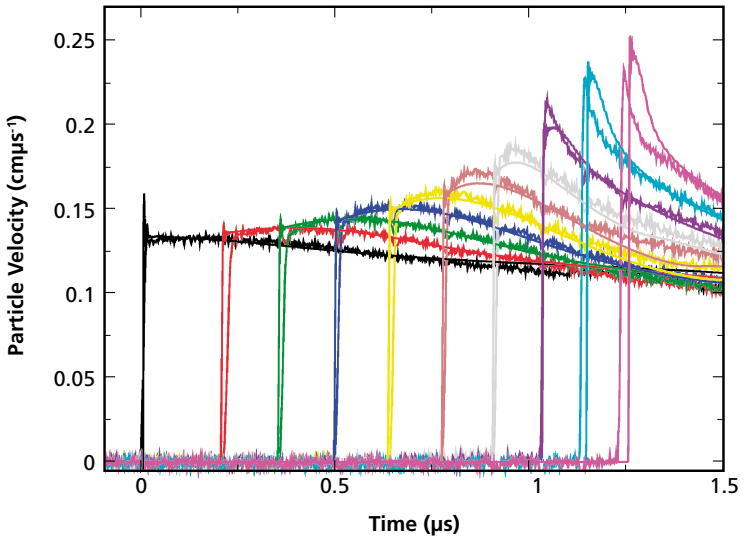

CREST fitted to PBX9502 experiments with initial shock amplitudes ranging from 10.64 - 16.27 GPa. A typical fit in this range, CREST has smoothed the curves.

FIGURE 5

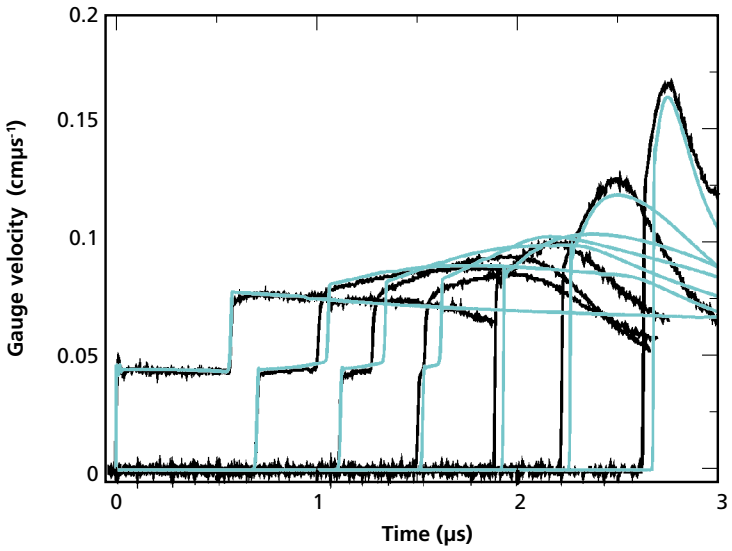

Comparison of CREST in-material gauge traces (green) with experimental results (black) for doubly-shocked EDC37.

cope with the effect that the second shock has on the reaction rate. Without this additional criterion pressure based reaction rates would predict that the detonation would occur far too quickly after the arrival of the second shock.

The second example shows the way CREST deals with porosity in an explosive. The CREST model for PBX9502 was used to simulate LX-17 experiments with varying porosity, because the two explosives are similar to each other in composition. Figure 6 compares the CREST results with experimental data. The error bars on the CREST results highlight the uncertainty in the exact position of the transition to detonation. Without changing parameter values CREST also gives a good fit to a 7% porosity Pop Plot for LX-17. The change in porosity is fully accounted for in CREST by using a porosity model in the unreacted equation of state and no changes have to be made to the reaction rate coefficients. Pressure based models are unable to predict this effect without changing the reaction rate coefficients.

The third example shows how CREST can also deal with changes in the initial temperature of the explosive. Only the initial density and internal energy, of the unreacted material, have to be adjusted in order to correctly set the initial state of the explosive at appropriate starting temperatures. Figure 7 shows that CREST captures the trends of the changes to the Pop Plot when compared to PBX9502 experimental data over a range of initial temperatures from -55 to +75 °C. Pressure based models would show almost no effect due to temperature without changing the reaction coefficients.

CREST and Predictions of Detonation Propagation

CREST was originally developed to simulate the growth of shock waves as they transform into a detonation. The structure of a fully formed detonation wave allows the view that detonations

FIGURE 6

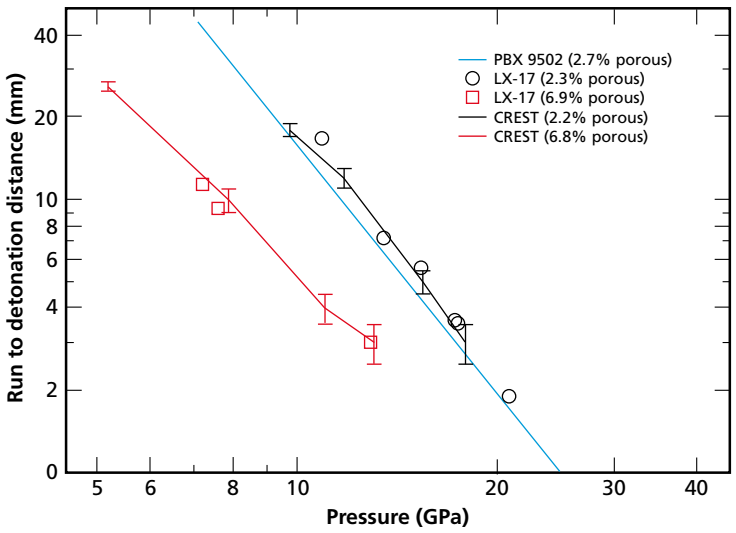

CREST predictions compared to porous experimental results.

are just an extreme example of this behaviour. The detonation front has a leading inert shock wave that travels into the undisturbed explosive and triggers reactions in the region immediately behind the wave.

The mechanics of the reaction growth in this region can be considered as being no different to those seen behind lower amplitude shocks. Only the immediate outcome is different because in detonation waves the reaction nearly always grows to completion behind the leading inert shock and the reaction zone structure is stable over time.

If a powerful computer is used to resolve the reaction zone then CREST can predict detonation propagation effects using the same reaction coefficients, and with the same model, as used in predicting the reaction growth. Three examples are discussed where CREST has been used to model detonations at or near the boundary of detonation failure. This is typically a difficult region to model.

The first example is of an initially overdriven detonation introduced into a cylinder of PBX9502 that is below its failure diameter. Figure 8 shows the pressure plots obtained using CREST. There is a slow fading of the detonation as it proceeds along the cylinder. CREST predicts a failure diameter of just less than 8 mm while the experimental result lies in the region of 7.5-8.0 mm.

FIGURE 7

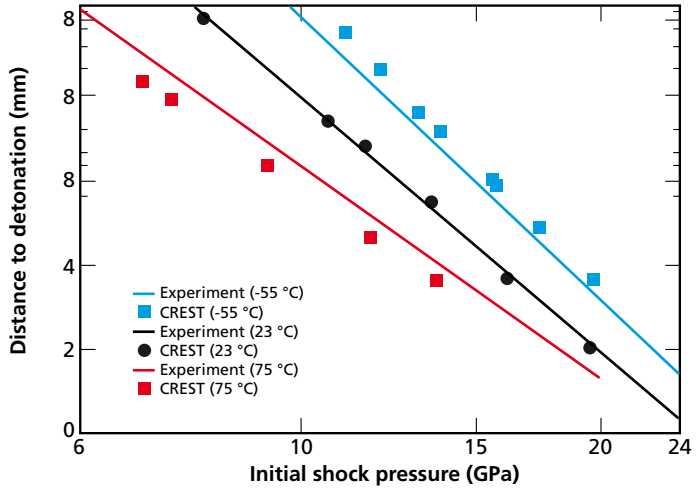

CREST simulations comparing Pop Plot predictions with experiments on PBX9502 at different initial temperatures.

FIGURE 8

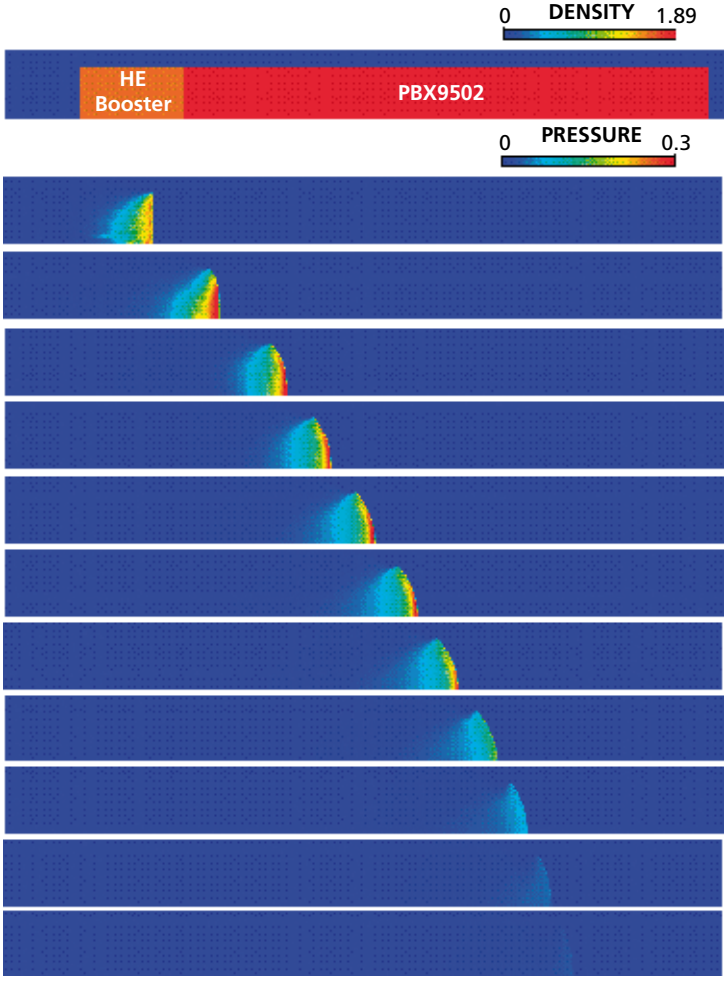

Pressure plots from a CREST simulation of a shock wave in cylinder of PBX9502. Shown as a series of snap shots, increasing in time from top to bottom.

FIGURE 9

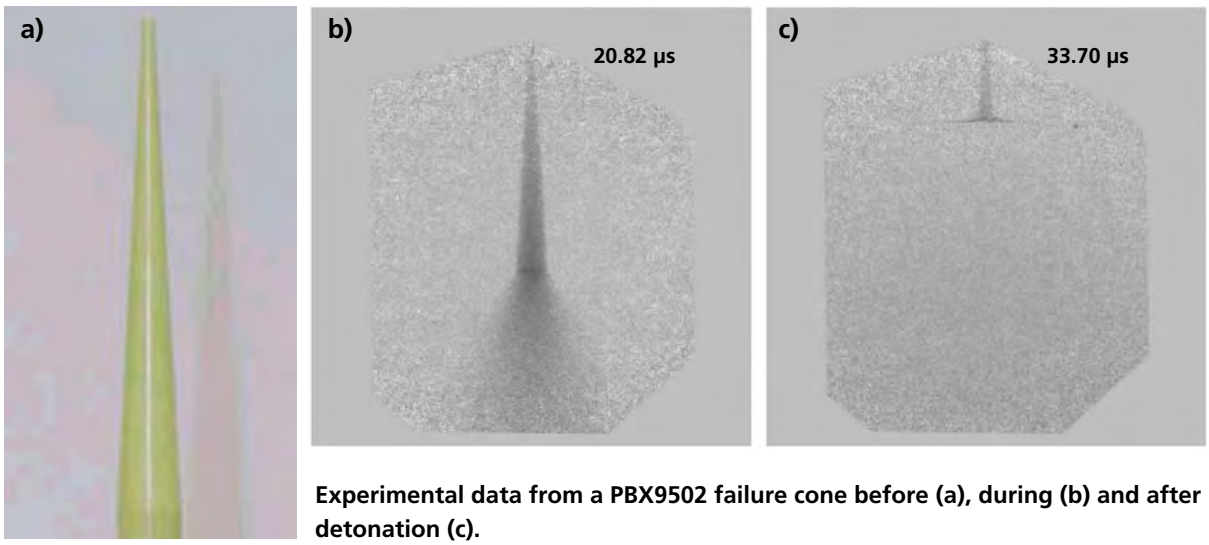

Experimental data from a PBX9502 failure cone before (a), during (b) and after detonation (c).

The detonation fades because the release waves from the charge surface weaken the leading shock in the detonation, first at the edge of the charge and then progressively inwards. The detonation fails on axis when the leading shock strength is below the absolute initiation threshold.

The detonation front is shown slowing and becoming increasingly curved before fading to a non-reactive shock wave.

The second example is of dynamic detonation failure in a cone. Predicting the exact point of failure is difficult because not only is the detonation fading but its inertia will propel it into smaller charge diameters than would support a steady detonation in a cylindrical geometry. The explosive used in this experiment was PBX9502. Figure 9 shows the explosive cone before the experiment (a) and x-rays during detonation (b) and after the detonation has failed (c).

FIGURE 10

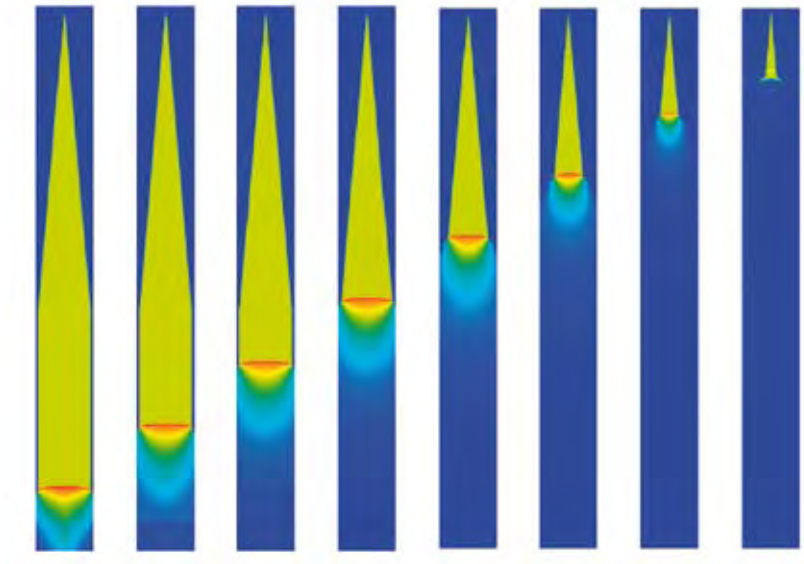

Density contours from the CREST simulation of a PBX9502 failure cone.

Figure 10 shows the CREST simulation of the example. The shape and size of the remaining explosive, after the propagation of the detonation, calculated by CREST is very close to that of the experiments, see Figure 9c.

The third example shows how CREST can be used to model detonations around sharp corners. When a detonation wave turns a sharp corner regions of unreacted or partly reacted explosive are left. Figure 11 shows the setup of this experiment with PMMA and aluminium (Al). Figures 12 and 13 show X-rays of the experiment

and results from the CREST simulations. Figure 12 is from experiments with the PMMA block and Figure 13 of the Al block. Areas of unreacted or partially reacted explosive are referred to as 'dead zones'.

The shock wave induced into the PMMA block is slower to cross the PMMA than the detonation front is in travelling around the corner. Hence the dead zone is only due to the corner turning properties of the explosive. The Al block transmits the shock wave faster than the detonation front can turn the corner, resulting in part of the explosive being pre-shocked before the detonation wave arrives. Here the dead zone is a combination of corner turning and desensitization of the explosive by the shock transmitted through the Al. CREST shows itself quite capable of predicting such phenomena without recourse to the "desensitization" criteria needed by many other reaction rate models.

Conclusions

CREST has shown a remarkable ability to predict shock wave initiation and detonation phenomena. It has been tested successfully in a 2D adaptive mesh refinement hydrocode which will allow a greater range of problems to be tackled with existing computer resources.

CREST is a continuum-based model and so phenomena that are rooted in the explosive's morphology e.g. grain size effects are beyond its capability. Other

FIGURE 11

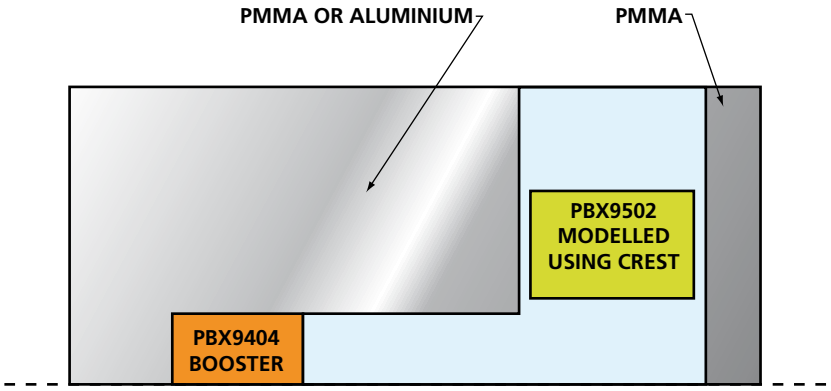

Corner turning experiment.

FIGURE 12

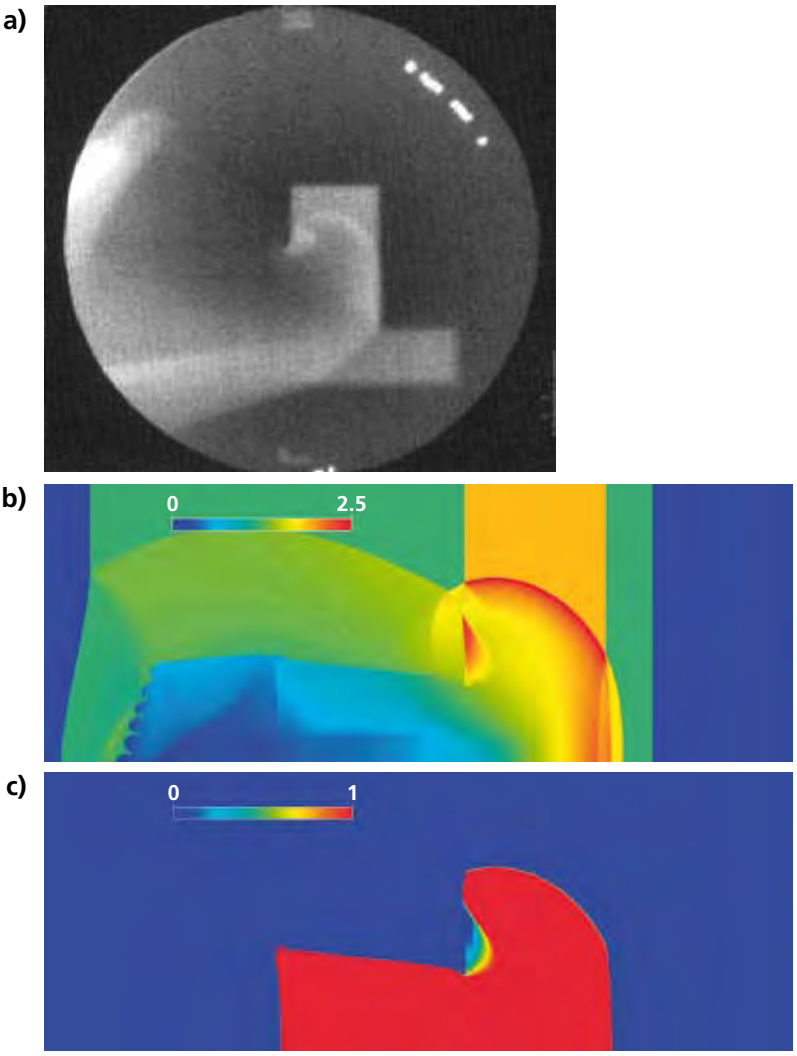

a) X-Ray of PMMA block experiment after corner turning. b) Density contours from CREST simulation. c) Burn fraction contours from CREST simulation.

codes have introduced such phenomena in a statistical fashion and further work is needed to see if CREST can be similarly adapted.

CREST already provides an important new predictive capability covering a large region of shock initiation and detonation propagation problems. The same reaction-rate coefficient values can be used over a range of initial porosities and temperatures for a given explosive. This reduces the need for large numbers of experiments to cover scenarios in which the explosive is exposed to wide ranges of temperature or has been damaged.

Acknowledgements

The CREST model has been developed and tested by the High Explosives Modelling team at AWE since 2004. The author would like to thank all members of the team, in particular Caroline Handley, Nick Whitworth and Brian Lambourn.

The author would like to thank Rick Gustavsen and co-workers at Los Alamos National Laboratories (LANL) both for conducting very high quality experiments on behalf of AWE and for allowing access to other data ahead of publication.

The author would like to thank Ron Winter, Peter Taylor, Sue Sorber and other past and present members of Hydro Dynamics team for their efforts in coordinating with LANL and for many useful discussions regarding the experiments and their results.

FIGURE 13

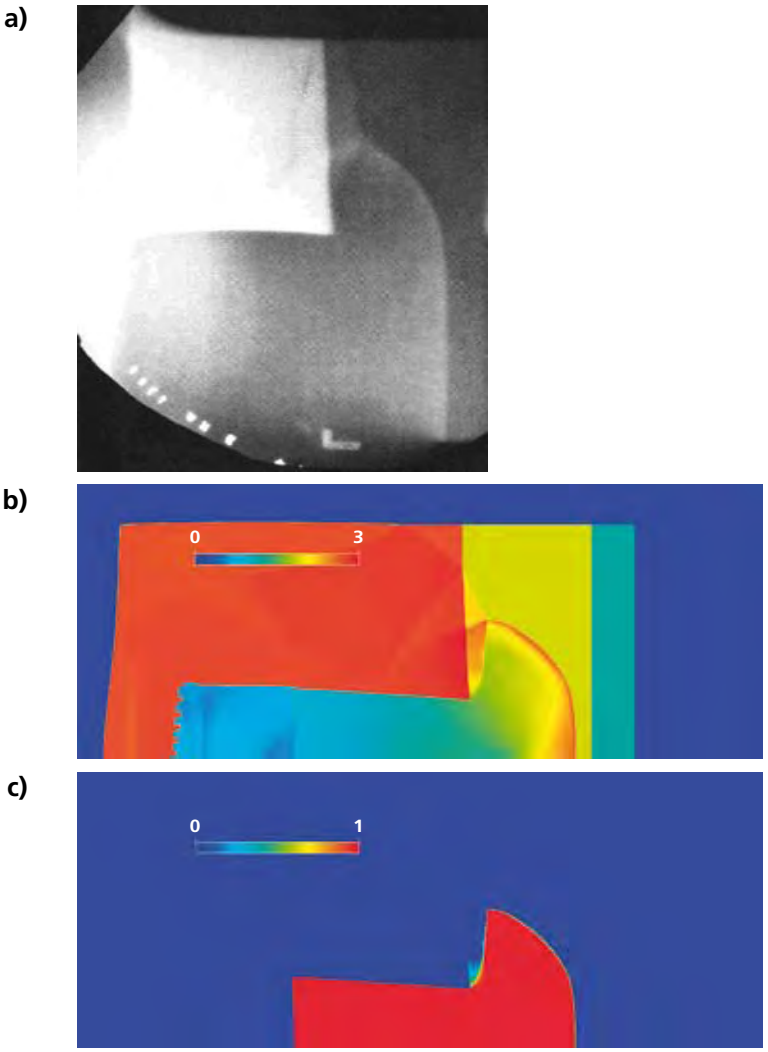

a) X-Ray of Al block for corner test. b) CREST simulation of density contours for Al block. c) CREST simulation of burn factor for Al block.

References

1 J Vorthman, G Andrews & J Wackerle, 8th Symposium (International) on Detonation, p99, Albuquerque, NM (1985).

2 H R James, B D Lambourn, Journal of Applied Physics, volume 100, 084906 (2006).

3 JB Ramsay & A Popolato, 4th Symposium (International) on Detonation, p233, Silver Spring MD (1965).

4 HR James, 13th International Detonation Symposium, p952, Norfolk, VA (2006).

BOX 1

Shock-to-Detonation Transition and its Measurement by In-material Gauges

Rather than having to heat the whole of a heterogeneous explosive to a point where it reacts, a shock wave interacts with the density discontinuities to form localised stress concentrations. These in turn act as localised heat sources or hotspots.

The hotspots activate explosive crystals in their vicinity to release their chemical energy over relatively small time scales. This energy increases the strength of the shock which in turn activates more hotspots on smaller timescales, and eventually the process can run away and the shock transits into a detonation.

In-material particle velocity gauges are embedded in the explosive. The motion of the metallic elements through an externally applied magnetic field, when the explosive is subjected to a shock wave, induces a voltage across the gauge elements. This voltage is related to the particle velocities within the material under measurement.

The thickness of the gauge package is about 60 μm of which 25 μm is aluminium. Each package consists of 10 to 12 gauge elements,[1] which are located at different depths in the explosive. The distance between elements is in the range of 0.5 to 1 mm.

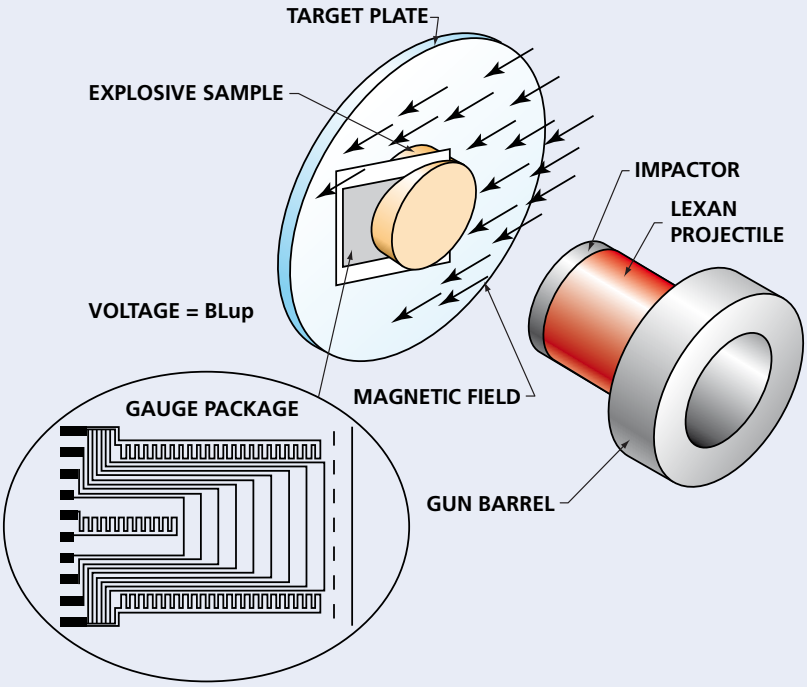

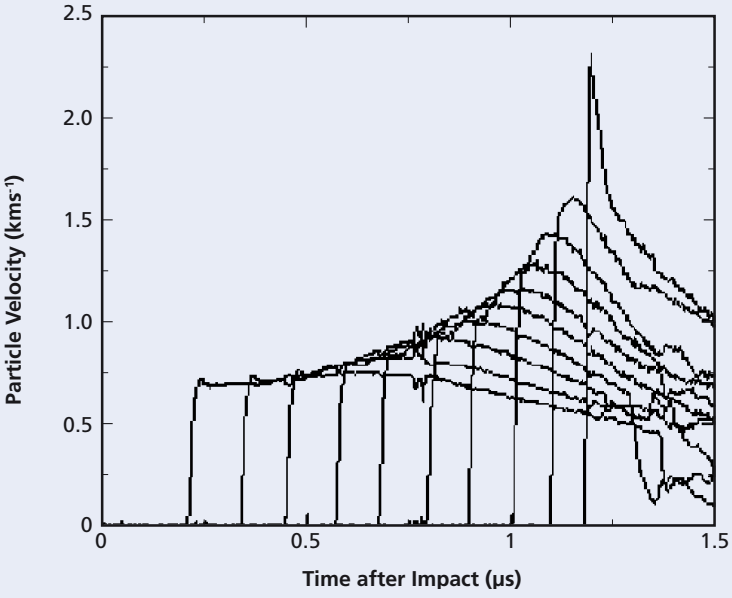

Each gauge trace originates from a metallic element at a given depth in the explosive. These traces show the behaviour of the flow at and behind the shock wave in the explosive. The shock is originally a flat-topped pulse but reaction in the flow behind the shock produces a "hump" that increases in amplitude with depth and eventually coalesces with the shock front to form a detonation wave.

BOX 2

Entropy and the CREST Reaction Rate

The particle velocity histories suggest that, at least to first order, the reaction rate behind a shock wave depends only on 'shock strength'.[2] Pressure, density or particle velocity can not be used to define reaction rate as they increase behind the shock due to the reaction. One variable that does not change behind the shock, at least in the way the CREST model is defined, is the entropy of the shocked but still unreacted element of the explosive.

Entropy is an appropriate parameter because it describes the state of disorder of the explosive structure after the shock has passed. The stronger the shock wave, the greater the extent of disorder and hence the greater the unreacted entropy. The greater the entropy the faster the reaction in the explosive proceeds.

The CREST reaction rate is written as the sum of three terms.

$$\dot{\lambda} = (1-\lambda)\left\{m_1 \dot{\lambda}_1 + m_2 \dot{\lambda}_2 + m_3 \dot{\lambda}_3\right\}$$

Where each term is dependent on the time since the shock passed (t).

$$\dot{\lambda}_1 = (1-\lambda_1)\, b_1 t$$
$$\dot{\lambda}_2 = (1-\lambda_2)\, \lambda_1\, b_2 t$$
$$\dot{\lambda}_3 = (1-\lambda_3)\, \lambda_1\, b_3 t$$

The parameters m and b depend on the entropy. λ is the mass fraction of reacted explosive at any given position in space and time within the explosive.

The reaction rate equations are integrated and each reaction rate is written in terms of the extent of reaction and the coefficients b_1, b_2 and b_3. For all explosives there is a minimum shock wave strength (the absolute shock threshold) below which no reaction takes place. This is built into the dependence of the parameters on entropy.

BOX 3

Pop Plots and the Initiation Threshold.

The Pop Plot, named after Alphonse Popolato,[3] expresses a unique relationship between the initial sustained shock pressure and the time or distance to detonation within a given explosive. The classic Pop Plot gives a linear relationship in log-log space as shown below for PBX9502. Investigation[4] showed that Pop Plots with either concave or convex curvatures are also possible for some types of explosive morphology. The Pop Plot for an explosive depends on the initial porosity and temperature of the material.

The Pop Plot for an explosive gives the minimum distance for a shock wave to run to detonation, for a given initial impact pressure. If the shock is created by the impact of a thin flyer, then below a certain flyer thickness (L_0) the shock can no longer be considered as sustained and the run distance to detonation increases. This can tend to very long distances compared to the original Pop Plot when the flyer thickness approaches the initiation threshold. Below this threshold thickness shock-induced detonations do not occur. At the other end of the scale, for flyer thicknesses above L_0, the run distance remains constant for a given pressure.

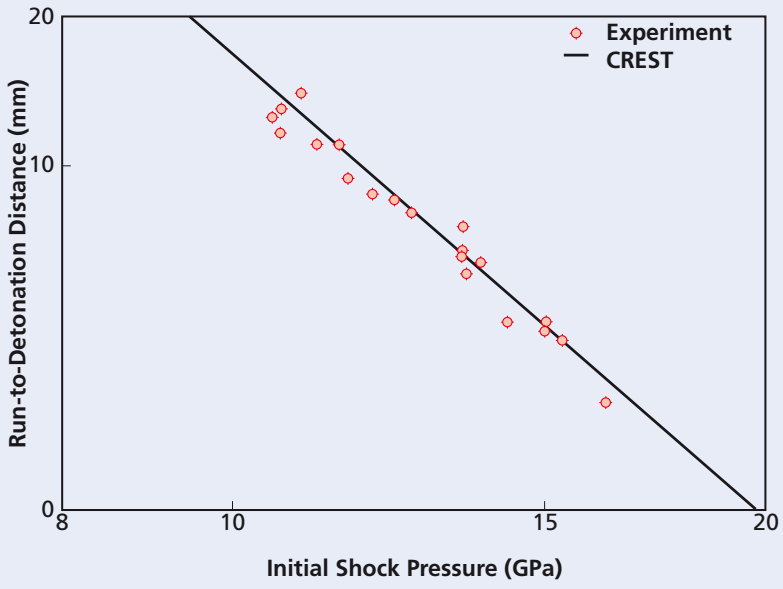

Pop Plot for PBX9502 obtained from in-material gauges at ambient temperature.

Hugh James can be contacted on e-mail: hugh.james@awe.co.uk

Hugh James • Hugh joined AWRE, Foulness at the age of 18. A shift in interest from experimental to theoretical work led to Hugh heading the Theoretical and Computing Section at Foulness in 1986. He became involved on International Collaborative work on explosives and holds two of the prestigious TTCP (The Technical Cooperation Programme) Achievement Awards. Hugh moved to Aldermaston in 1995 and was promoted to Distinguished Scientist in 2006. He was awarded an MBE in the Queen's Birthday Honours List in 2008 for services to the Defence Industry. He currently works with a highly talented team responsible for developing models of the dynamic behaviour of explosives when subjected to extreme conditions.

Random Particle Simulation

AWE invests much effort into developing particle based codes to simulate specific transport phenomena over a range of distances and timescales. The phenomena simulated vary from X-ray scattering to the settlement of debris after an explosion.

This article presents work undertaken at AWE on random particle methods, called Monte Carlo methods after the famous casino. The introduction draws contrasts and comparisons with other conventional methods for modelling transport phenomena. Some analysis against real test data is also presented.

Unless a physical transport problem exhibits some obvious collective behaviour e.g. an oscillation, in a computer model it is often convenient to represent a field by an ensemble of semi-classical super particles. These super particles drift through space according to simple classical trajectories. They also experience physical (quantum) scattering into new states at seemingly random times, as if dice had been rolled to determine their fate. By using computer generated pseudo-random numbers to 'roll the dice' and generate the fate of each particle and by gathering individual flight histories over a succession of iterations, a representative picture of the field is established.

Monte Carlo particle simulations have at their foundation some particular form of the Boltzmann Transport Equation, see Box 1. This relates the rate of change of the particle distribution, in both real and momentum space, to the directional flow of particles and the rates at which particles are scattered from one momentum state to another.

Even with comparatively simple laws to describe the particle dynamics e.g. scattering problems that have simple sources or boundary conditions, the fact that the Boltzmann Transport Equation tends to involve integral as well as differential operators means that only idealised situations produce an analytic solution.

In real applications issues such as time-dependent energy sources, the need to describe the expansion of heated material and multi-group effects mean that even a semi-analytic result is not possible, unless the transport is simplified.[1] Moreover, the transport equation must usually be coupled to a balance equation of some kind. Examples of balance equations include energy exchange with the material for thermal photons, Poisson's equation for the electric field in systems with mobile as well as fixed charges and Schrödinger's equation for quantum confined charges.[2]

Influenced by the computer resources of the time the Boltzmann Transport Equation ascribed to a particular problem had to be approximated in some way. This meant abandoning certain detail about the distribution function. Generally this was done by taking moments of the operators e.g. integration over direction, in order to arrive at a diffusion equation. Directional information about the distribution function is lost, leaving behind an equation which describes a density e.g. charge or energy, rather than intensity.

A deterministic route of this kind may be sufficient to model heat spreading across an opaque medium or mobile electrons driven through a semiconductor crystal at low fields ($<10^5$ Vm^{-1}). It is not suitable for heat transfer problems that include free streaming as well as diffuse behaviour nor can it describe hot-electron effects in the presence of high, often transient, electric fields ($>10^7$ Vm^{-1}).

An alternative approach is to preserve the transport operators and make a compromise with the distribution function. One route is to collapse the function onto a set of distinct directions. This is the basis of a deterministic discrete ordinates scheme, referred to as the Sn method.[3]

The other path is to represent the distribution function stochastically. This is the basis for the Monte Carlo method. It has the potential advantage that the whole of the relevant phase space can be sampled. There is an evident pitfall in that if just a few particles are used to approximate for the distribution function at any time, then the variance in the numerical result can be great. With modern supercomputers a large number of small-ensemble

calculations can be run in parallel, on many processors, and their outputs gathered to produce a collective result with improved statistics.

While there is a disadvantage in terms of statistical noise with a Monte Carlo method one advantage is that it offers good scalability. It is possible to balance the workload between processors, so that the run-time for a given calculation is reduced in proportion to the number of processors used. Because of their particular merits in certain circumstances and also as comparative models, both deterministic and Monte Carlo transport codes are developed by AWE.

Comparison of Approaches

A number of tests have been used to compare the different models with each other and also with experimental data. One such experiment is the laser driven asymmetric collapse of a glass bubble. In this study, by the Plasma Physics Department, the Monte Carlo and Sn methods were run in conjunction with a 2D Lagrangian-ALE hydrodynamic code.

Suspended centrally within a gold hohlraum was a 600 μm diameter hollow sphere consisting of a 3 μm thick glass shell coated with a 30 μm deep plastic ablator. The hohlraum was heated on one side only by focused laser beams, the laser pulse lasted 1.6 ns and delivered 6.2 kJ of energy. The plastic hemisphere on the driven side

FIGURE 1

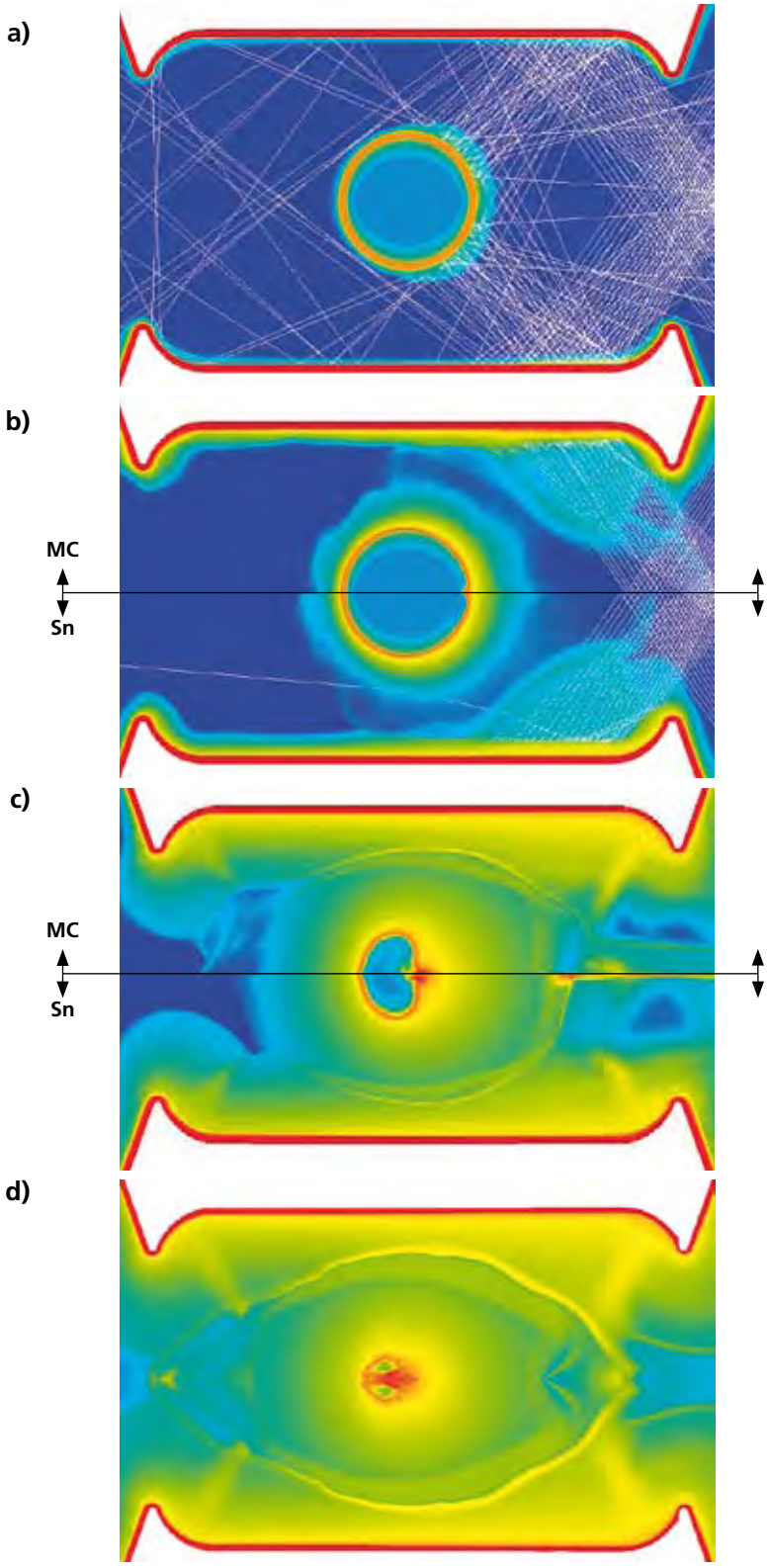

Logarithmic plots of mass density for the laser driven asymmetric collapse of a glass bubble. a) Monte Carlo plot at 0.2 ns. b) Monte Carlo and Sn plot at 0.8 ns. c) Monte Carlo and Sn plot at 2.7 ns. d) Monte Carlo plot at 3.5 ns.

was preferentially heated by X-rays that were radiated from the hohlraum, causing it to ablate more strongly. Gold does not absorb perfectly and at early times patches of the plastic ablator were also illuminated by rays deflected off the hohlraum wall. Figure 1 shows mass density plots from the simulations. In Figure 1a and 1b the densely packed white lines represent the laser source from the right hand edge. The upper half of Figure 1c is taken from the Monte Carlo simulation and the lower half from a Sn model.

According to both calculations, by 1 ns the ablating plastic collides with gold ablating off the hohlraum wall. Where the fronts collide a ribbon of plasma is heated above 5 keV. In the subsequent coasting phase that follows the laser pulse, the driven hemisphere of the glass bubble collapses onto the hohlraum axis. This forms a plug of material which eventually punctures the quiet hemisphere.

Radiographs taken through a porthole in the side of the hohlraum cylinder recorded the bubble collapse. Figure 2a and 2b show radiographs at time 3 ns and 3.7 ns respectively. Figures 2c and 2d show magnified density plots at times 2.7 ns and 3.5 ns. The effective temperature of the hohlraum was 0.20 to 0.21 keV, the inferred temperature was 0.18 to 0.19 keV.

Such was the ablation of the gold and plastic that material was expelled through the laser beam entry hole. There is strong shear flow at the plastic-gold interface.

This application proved to be a stringent test for the 2D Lagrangian-ALE re-meshing algorithm in the hydrocode and of the Monte Carlo particle tracking and re-mapping on the distorting mesh.

Both the Sn and Monte Carlo transport models predicted an evolution in the shape of the glass bubble during its collapse that is similar to the radiography. The simulations also predicted an on-axis collapse that is in advance of that measured from the experiment. There is presently no separation of electron and ion temperatures, which may account for the time differences.

By making use of improved compatible hydrodynamics[4] and using cell-by-cell rather than regional ALE, it has been possible to run simulations of this kind from start to finish without needing to break the calculation and link to another hydrodynamics code. Previously such a calculation would start in the Lagrangian frame and once the mesh had tangled, some time later, it would be linked and completed on an Eulerian mesh. This would result in a loss of resolution.

Implicit Monte Carlo Radiation Transport

If a thermal radiation transport calculation is to be self-consistent and stable it is important to account for the simultaneous absorption and re-emission of photons by the heated materials. For each iteration it is necessary to

FIGURE 2

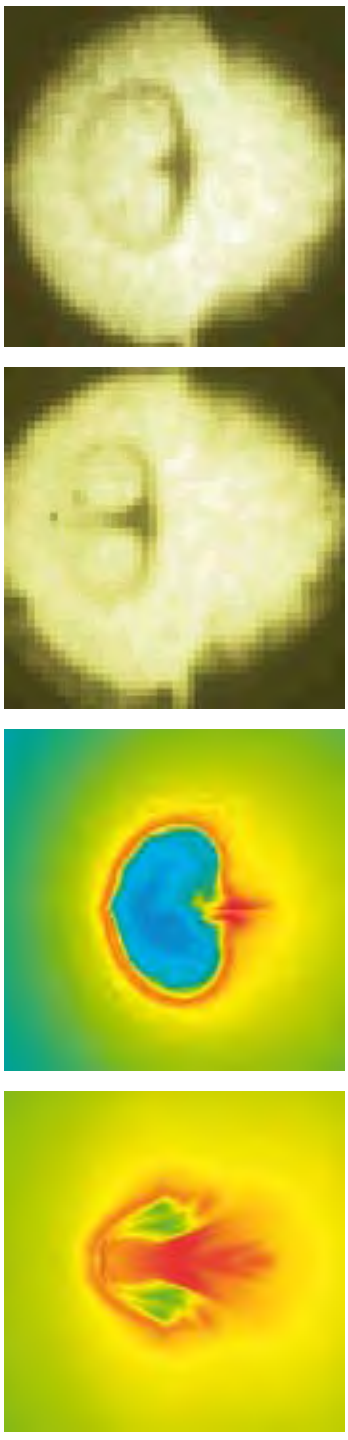

Images of hohlraum and glass bubble at different times. a) Experimental radiograph at 3 ns. b) Experimental radiograph at 3.7 ns. c) Magnified density plot of bubble collapse at 2.7 ns. d) Magnified density plot of bubble collapse at 3.5 ns.

"Mesh resolution is a significant issue for radiation transport problems, in particular for implicit Monte Carlo calculations. "

project forward what the re-emissive strength of each participating cell should be. Without such a projection the coupled solution of the photon transport and energy balance with the surroundings is said to be explicit. This tends to give an unstable result unless the time step is particularly short e.g. 10^{-14} seconds. An explicit calculation requires short time steps to be maintained throughout.

Implicit schemes have the potential advantage that the restriction on the time step can be relaxed, with the time step steadily raised as the problem approaches thermal equilibrium. This may be sufficient for problems that involve participating yet static media. Unfortunately it is not always appropriate for radiation hydrodynamic problems.

A key step towards numerically stable radiation transport calculations was made by Fleck and Cummings.[5] They identified that an artificial pseudo-scattering process could be used as a simple yet effective way of representing the balance between the absorption and spontaneous re-emission of radiation within a time step. A reduced absorption opacity ($f\sigma$) was prescribed, where f is the dimensionless Fleck parameter ($0 < f < 1$) and σ is the absorption opacity. The arbitrary re-emission was represented by the isotropic scattering of particles at a rate $c(1-f)\sigma$, where c is the speed of light.

There can be occasions when the net absorption is minimal but the mean free path is still short e.g. a medium that is hot yet opaque. Implicit particle tracking can then be computationally expensive, pseudo-scattering events dominate and the transport becomes diffusive.

Fleck and Canfield[6] provided a solution to this problem by introducing a time-saving random walk algorithm. This is based on the probability that a particle is within a given radius (R) after a time (Δt). Rather than track a particle over successive short flights a selection from a set of probability distributions can be made.

For the random walk approximation to be valid, the implicit transport time step (Δt) should exceed the time that it would take for an asymptotic spatial distribution of similar particles, all with the same starting position, to be established. A useful rule-of-thumb is

$$\Delta t > \frac{R^2}{c\lambda} \quad (1)$$

Where λ is the optical mean free path, c the speed of light and R the prescribed radius.

The inclusion of a frequency dependent opacity introduces an extra degree of freedom. The random walk shows characteristics of both streaming and diffusion behaviour, as particles switch at random between states of comparatively long and short mean free path.

Central to any Monte Carlo particle simulation is the need to determine the time interval to the next scattering event. The method for calculating this is shown in Box 2. It may seem awkward to generate a stochastic free flight time if the total scattering rate was a function of the particle momentum **p**, because of the need to integrate the scattering rate $\Gamma(\mathbf{p}(t))$ with respect to time t. This is overcome by capping the total scattering rate to some realistic maximum, thus rendering it time-independent.

By making such a simplification the discrepancy between the total physical scattering rate at a given energy and the imposed ceiling can be thought of as being equivalent to a null or self-scattering process. Should the null process be chosen then no change is made to the particle other than its next random flight time is

generated. This simplifies the representation of the underlying physics, making the solution more tractable, but can compromise computational efficiency.

Graziani's Top Hat Problem

Mean free path zoning is desirable for radiation transport problems. This puts tough constraints on a hydrodynamic model and can require a prohibitive amount of computer memory. The need to make a compromise generally falls in favour of the host hydrocode, with the domain meshed accordingly.

Mesh resolution is a significant issue for radiation transport problems, in particular for implicit Monte Carlo calculations. In problems that involve radiating surfaces it is important to obtain an accurate representation of the albedo. If a mesh is not sufficiently fine then the energy absorbed from tracked particles will be distributed across too large a volume of material. This results in a weaker radiating material. Graziani's Top Hat problem[7] is a useful test with which to demonstrate the impact of coarse zoning. The modelled domain has an axial geometry consisting of a 2 cm radius by 7 cm long cylinder of opaque material. The cylinder has a constant opacity of 2000 cm^{-1}. Within the cylinder is inscribed a crooked pipe that resembles a top hat in plan view. The pipe is quite transparent to radiation, having a fixed opacity of just 0.2 cm^{-1}. The background temperature of the problem is 0.05 keV at the start and a constant Planckian source at 0.5 keV radiates particles into one end of the pipe. All boundaries at the edge of the mesh can lose particles that cross them, there is no reflection back into the domain.

The objective is to obtain a mesh-converged result for temperature-time histories at five

FIGURE 3

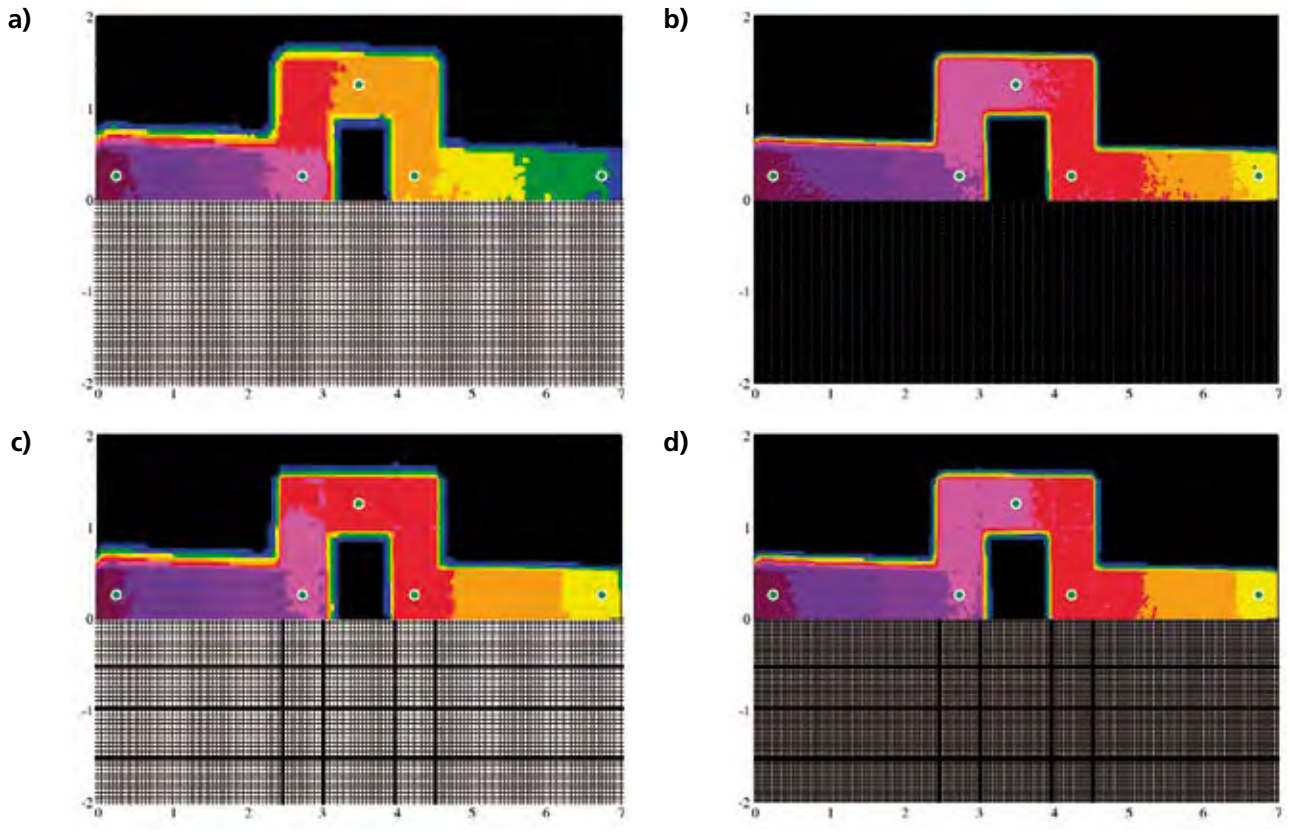

Coloured plots of Graziani's Top Hat problem at 1 μs. a) Regular grid mesh with 100 mean free paths across each cell. b) Regular grid mesh with 25 mean free paths across each cell. c) Geometrically zoned grid with 0.5 mean free paths zoning along pipe walls. d) Geometrically zoned grid with 0.25 mean free paths zoning along pipe walls.

recording stations displaced along the pipe section, four close to the axis of rotation and one off-axis at its mid-section. If the problem is run as prescribed, no result will in fact be time-converged because the initial time step of 10^{-11} seconds is multiplied by 1.1 at successive iterations, until it reaches a ceiling time step of 10^{-8} seconds. This does mean that only around 200 iterations need to be covered for 2 μs of transport to be simulated.

Figure 3 shows a comparison of material temperature contours at 1 μs for four different meshes. Figure 3c and 3d are geometrically zoned with mean free path zoning along the pipe wall of 0.5 and 0.25 respectively. This is intended to give a numerical result that is almost mesh-converged. Figure 3a and 3b are regular grids with 25 and 100 mean free path zones. Each coloured band represents a 10% range of the 0.5 keV constant source applied at the left-hand side of the pipe. The green markers along the pipe indicate stations at which the temperature is recorded over time.

Figure 4 shows the temperature results at each of the five stations along the pipe section in Graziani's Top Hat test. Using geometric zoning, that provides sub mean free path resolution along the pipe walls, a consistent set of temperature-time profiles is obtained indicating that result is close to being mesh-converged, shown in Figure 4a.

By contrast, the temperature-time histories obtained using the regular grids with coarse zones

FIGURE 4

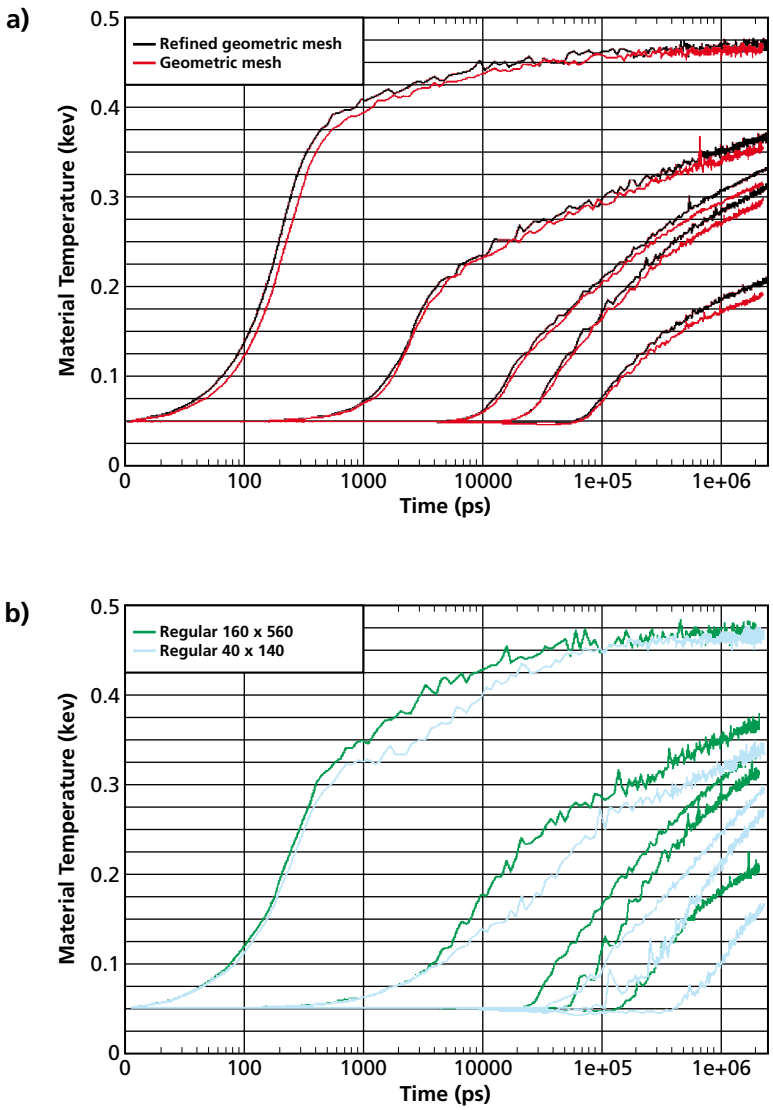

Temperature results from Grazianis Top Hat tests

have led to unwanted teleportation of energy into the cladding at early times, shown in Figure 4b. This has compromised the heating up of the five stations.

Developments

The Implicit Monte Carlo particle scheme, as set out by Fleck and Cummings,[5] is a valuable means of modelling radiation transport in multi-material hydrodynamic problems. It has the disadvantage that the variance of local radiation, hence material temperature, does not diminish as the problem approaches thermal equilibrium.

In recent years, there has been an effort to arrive at improved Monte Carlo methods for radiation

transport. One such scheme is of particular interest because it has the potential to produce answers of inherently lower variance.[8] This method solves for the difference between the radiation intensity (I_v) and the local black body field (B_v) and not the conventional intensity. The transport equation for thermal photons then takes the form:

$$\frac{dD_v}{dt} + c\boldsymbol{\Omega}.\text{grad}D_v + c\sigma_v D_v + \frac{dB_v}{dt} + c\boldsymbol{\Omega}.\text{grad}B_v = 0 \quad (2)$$

where D_v is the difference field, c is the speed of light, $\boldsymbol{\Omega}$ is the direction of travel and σ_v is the opacity.

While the difference field propagates and is absorbed like the radiation intensity, there is no pseudo-scattering only true absorption. The emission function ($\sigma_v B_v$) has been replaced by temporal and spatial derivatives of the local black body field (B_v). Radiation is sourced where there are significant temperature gradients and not in situations close to thermal equilibrium, for which D_v is approximately 0.

This implies that during the latter stages of a calculation there ought to be a reduction in the particle tracking work, not convergence towards a consistent high level of sourcing and tracking that is observed for conventional Implicit transport methods. Although reported at some length for 1D slab geometries, the merits of this scheme and related symbolic methods[9] for more general application in 2D or 3D has yet to be demonstrated. Effort is under way to do this.

At AWE there has been a strategy of developing generic deterministic or Monte Carlo transport packages that are readily interfaced with different (Eulerian or Lagrangian, 2D or 3D) host hydrodynamics codes. These are also more portable between computer architectures. Further improvements will be made to these models and new particle based models for different phenomena will also be explored.

Acknowledgments

The author would like to thank Mark Stevenson of the Plasma Physics Department at AWE for providing Figures 1 and 2 and also colleagues in the Design Physics Department at AWE.

References

1 R.B.Lowrie and J.D.Edwards *Shock Waves* 2008
2 G.C.Crow and R.A.Abram *Semicond. Sci. Technol.* **14** p721 1999
3 M.Modest *'Radiative Heat Transfer'* Springer 2nd ed. 2003
4 A.J.Barlow *Int. J. Numer. Meth. Fluids* **56** p953 2008
5 J.A.Fleck and J.D.Cummings, *Journ. Comput. Phys.* **8** p313 1971
6 J.A.Fleck and E.H.Canfield *Journ. Comput. Phys.* **54** p508 1984
7 N.A.Gentile *Journ. Comput. Phys.* **172** p543 2001
8 E.D.Brooks III, A.Szoke and J.D.L.Peterson *Journ. Comput. Phys.* **220** p471 2006
9 R.P.Smedley-Stevenson *'A linear SIMC scheme suitable for extension to multidimensions', Proceedings of the International Conference on Mathematics, Computational Methods and Reactor Physics* 2009

BOX 1

Boltzmann Transport Equation

The Boltzmann Transport Equation may be expressed generally as:

$$\frac{df}{dt} = -\boldsymbol{v}.\nabla_x f - \frac{d\,\boldsymbol{p}}{dt}\nabla_p f + \frac{df}{dt_{collisions}}$$

where the distribution function $f = f(\mathbf{r},\boldsymbol{p},t)$, $\mathbf{r}$ being the position vector, $\boldsymbol{p}$ being the momentum, and t the time. The first operator on the right hand side of the equation amounts to a flux term, where $\boldsymbol{v}$ is the particle velocity, the second term accounts for acceleration, e.g. under the influence of electromagnetic fields, and the third term represents collisions in and out of momentum $\boldsymbol{p}$.

Written specifically for thermal radiation, distribution function f is more usually thought of as the light intensity $I = I(\mathbf{r},\boldsymbol{\Omega},\nu,t)$, where $\boldsymbol{\Omega}$ is the direction of travel and ν the light frequency. By also allowing for the isotropic black body emission of radiation at points in space (but neglecting other photon sources and electron scattering), the Boltzmann Transport Equation for photons resembles:

Where c is the speed of light, σ_ν is the absorption per unit distance travelled, and B_ν is the black body function.

$$\frac{dI}{dt} = -c\boldsymbol{\Omega}.\nabla_x I - \sigma_\nu I + c\,\sigma_\nu \frac{B_\nu}{4\pi}$$

On the other hand, for mobile electrons (or holes) in a semiconductor crystal drawn by an applied electric field $\boldsymbol{E}$, in the absence of surface electrical contacts or localised traps, but in the presence of significant scattering by lattice vibrations and impurities, the transport equation takes the form:

$$\frac{dn}{dt} = -\boldsymbol{v}.\nabla_x n - \frac{q}{h}\boldsymbol{E}.\nabla_p n + \sum [n(\boldsymbol{r},\boldsymbol{k}',t)\,R(\boldsymbol{k}',\boldsymbol{k}) - n(\boldsymbol{r},\boldsymbol{k},t)\,R(\boldsymbol{k},\boldsymbol{k}')]$$

Where $n = n(\mathbf{r},\boldsymbol{k},t)$ is the density or particles with crystal momentum $\boldsymbol{k}$, $\boldsymbol{v}$ is the group velocity associated with $\boldsymbol{k}$ (derived from some knowledge of the electronic band structure), q the electron (or hole) charge, $\boldsymbol{E}(\mathbf{r},t)$ the electric field. The last term on the right hand side of the equation is the sum of all the possible scattering events to and from state $\boldsymbol{k}$, with these rates R generally obtained using Fermi's Golden Rule.

BOX 2

Monte Carlo Scattering Time

Consider a particle moving with momentum $\mathbf{p}$ at time t_j, for which the scattering rate is

$$\Gamma_j = \Gamma(\mathbf{p}(t_j))$$

The chance of scattering by time δt after t_j is

$$\Gamma_j \, \delta t$$

Conversely the probability of not scattering is

$$1 - \Gamma_j \, \delta t$$

If the local clock for this particle is reset, such that time $t = 0$ represents the time when the particle was last scattered, then the chance of flying freely for a time interval $t = 0$ to t_j, and then being scattered during the interval $\{t_j, t_j + \delta t\}$ is the product of all previous time steps:

$$P_j \delta t = \Pi_{k=0}^{j-1} [1 - \Gamma_\kappa \delta t] \, \Gamma_j \delta t$$

Hence

$$\ln(P_j \delta t) = \ln(\Gamma_j \delta t) - \Sigma_{k=0}^{j-1} \Gamma_\kappa \delta t.$$

If δt is small, such that the above equation can be transformed from a discrete to a continuous variable definition, then the probability of drifting for a time t, then being scattered within dt after that is:

$$P(t)dt = \Gamma(\mathbf{p}(t))dt \, e^{-\int_0^t \Gamma(\mathbf{p}(t'))dt'}$$

The particle is bound to scatter eventually, hence

$$\int_0^\infty P(t).dt = 1$$

If a flat random number r on the interval $\{0,1\}$ were to correspond to some time τ_r at which the particle scatters, then

$$r = \int_0^{\tau_r} e^{-\int_0^t \Gamma(\mathbf{p}(t'))dt'} dt$$

Unless $\Gamma(\mathbf{p}(t))$ is a simple function, it is not straightforward to rearrange the above equation to express τ_r in terms of r.

If

$$\Gamma(\mathbf{p}(t)) = \gamma$$

where γ is a constant then a randomly generated free flight time is simply

$$\tau_r = -\frac{\ln(r)}{\gamma}$$

AUTHOR PROFILE

Gavin Crow can be contacted on e-mail: gavin.crow@awe.co.uk

Gavin Crow • Gavin read Physics at Durham University (BSc 1990, PhD 1994). He continued there with post doctoral research into the simulation of transport effects in semiconductor laser diodes (1993-1996) and silicon-germanium devices (1997-1999). Following an additional year as an undergraduate and postgraduate tutor, in 2000 he moved to the Corning Research Centre (formerly BT Research Laboratories, Martlesham). There, he investigated the possible beam steering application of planar photonic crystals. Further research on semiconductor optical amplifiers led to a set of design rules for achieving polarisation insensitivity; a patent co-authored with I. F. Lealman was granted in 2004. Gavin joined AWE's Computational Physics Group in autumn 2003, where he has since worked on the modelling of thermal radiation transport. He is a chartered physicist and member of the Institute of Physics.

Lightning Arrester Connectors

The lightning-arrester connector (LAC) has been an integral component of many external systems since the early 1970's. It protects sensitive electronic circuits by providing a short circuit to ground during an excessive voltage applied to one or more of the pins. Development of this component was prompted by a lightning strike on the Apollo 12 space craft.[1] Lightning is a serious hazard, even if a direct strike does not occur, a nearby strike can induce thousands of amps into equipment or fixtures.[2]

Protective devices of various types have proven effective in diverting lightning energy and preventing damage to structures and systems for the last thirty years or more. The development of the LAC has enabled a desired breakdown voltage to be set, whereupon the pin would become short circuited to the casing within microseconds of the over voltage occurring, but allowing normal voltages to pass unaffected.

This article presents experimentation and analysis on LACs. Initial work performed by Sandia National Laboratories, (SNL)[3-5] provided concepts of the lightning-arrester and data from tests performed on the modified multipin connector (MIL-C-27599 type I class H-hermetically sealed) which contained 18 to 32 pins with a solid sleeve of rutile (TiO_2) between the pins and the grounded web.

FIGURE 1

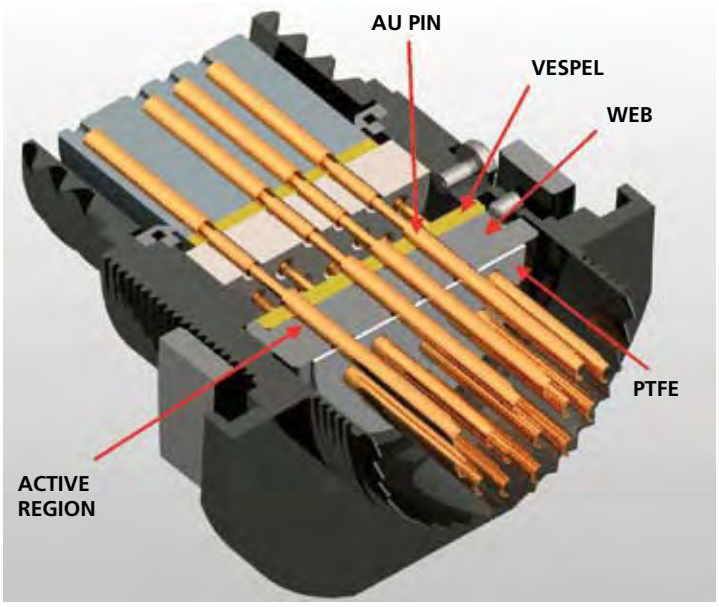

Sectioned LAC geometry indicating major components.

The LAC discussed in this article is a bespoke 26-pin device, shown in Figure 1. The pins are surrounded at distance by a stainless steel web, leaving a 250 μm 'air-gap', into which is inserted a ceramic dielectric 'trigger material'. The trigger material, in this case rutile, is believed to be the main catalyst in the diversion of the over voltage signals. The rutile is sintered, milled and sieved into approximately 150-180 μm sized particles. The material is held within the air-gap by the use of a polyimide (Vespal) disc on the female side and a PTFE disc on the opposite side of the LAC. The LAC is then sealed on the PTFE (male) side by Dymax 955, a UV setting epoxy resin.

The LACs discussed within this article were struck with an impulse wave form simulating a lightning strike in accordance with the ANSI standard designated D3426-97.[6] This involves lightning threat component 'A', which is the first return stroke of lightning flash. Some LACs were subjected to continuing current, component 'B' and 'C', threats.

The mean average breakdown voltage of the various web diameters and particle sizes is shown in Figure 2. The empty cavity denoted 'E' shows a breakdown voltage consistent with that predicted by Meek[7] and Lau.[8] The trend of the breakdown voltage with particle size with respect to the web diameter was found to be consistent. It is a high voltage for smaller particles, the lowest voltage is found when the

FIGURE 2

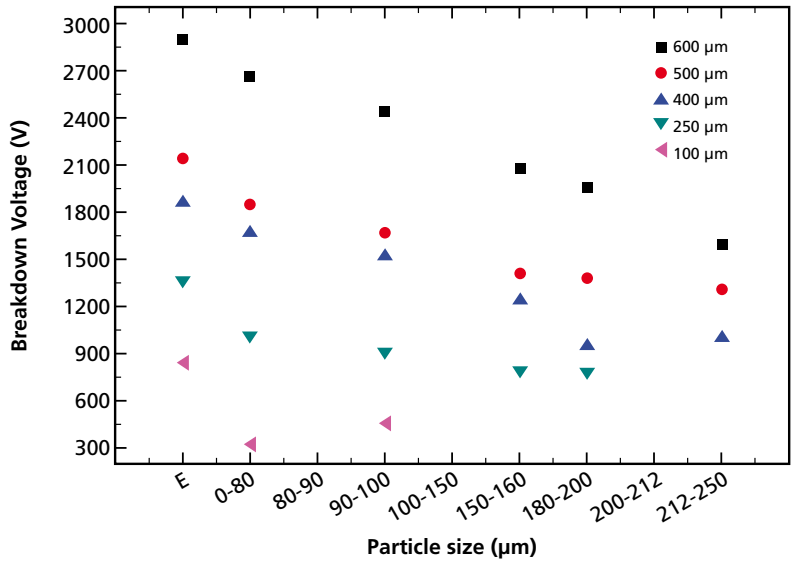

Breakdown voltage dependency upon particle size and air gap size (without chamfer).

air gap was twice the diameter of the particle size and the voltage rises again until only one particle can fit within the air gap.

Capacitance Measurements

The capacitance measurements of the pins were performed at a frequency of 20 kHz. Pins without trigger material were measured first to obtain the capacitance of the system. Once the trigger particles had been inserted the difference in capacitance would represent the permittivity of the rutile in the cavity alone. The breakdown tests were performed with a 5 kV impulse generator with a rise time of 0.5 kVμs^{-1} at ambient temperature.

Figure 3 displays the capacitance of the single pin LAC, again 'E' denotes the empty pin with no trigger particles. The formula for capacitance of a coaxial line is

$$C = \frac{24.1 \times \varepsilon_r}{Log_{10}\left(\frac{D}{d}\right)} \quad (1)$$

where D denotes the outer conductor diameter, d represents the inner conductor diameter and ε_r is the relative permittivity. The coaxial line length for the LAC can not be measured in isolation. The whole LAC system was measured and the differences observed between the empty LAC and the different particle diameters within the different web diameters. The results for the capacitance provide an explanation for the packaging of the particles in the air gap. Capacitance decreased as the particle size became greater due to increased edge effects arising from large particle stacking.

Figure 4 is a comparison of the theoretical capacitance with that measured for the empty LAC. The difference in the theoretical and measured capacitance can be attributed to stray capacitance, which on average can be approximated to 1.7 pF. Taking this as a constant value for all

FIGURE 3

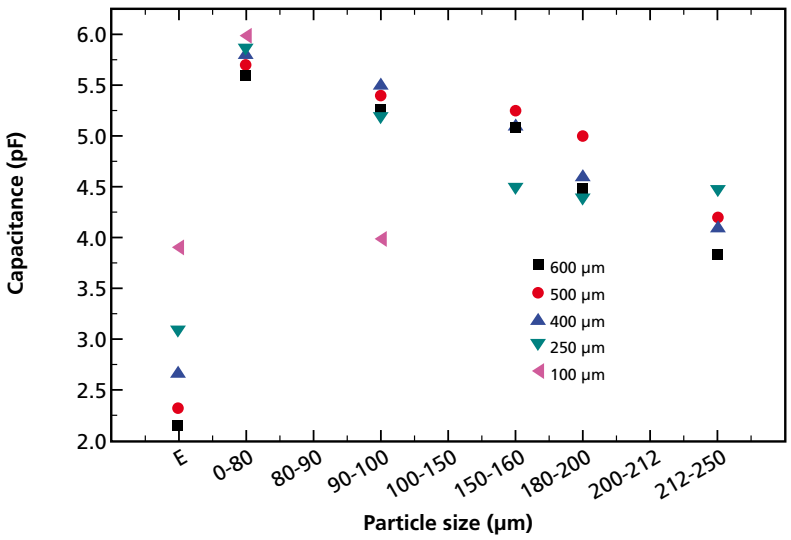

Capacitance dependency upon particle size and air gap size (without chamfer).

measurements the effective relative permittivity of the different particle loadings can be deduced and is shown in Figure 5. The effective relative permittivity increases with gap size and this can be interpreted as the volume fraction of particles increasing with gap size.

Connector Geometry

The LAC is designed with chamfers at the top and bottom of the web where the pins leave and enter. The chamfers ensure that the location of the breakdown of the rutile trigger particles occurs within the central area of the pin and web. The increased field at the chamfer may be causing the breakdown to occur at that location. The LACs tested and examined would also suggest that the breakdown occurred at the chamfer as there was damage found in this area.

FIGURE 4

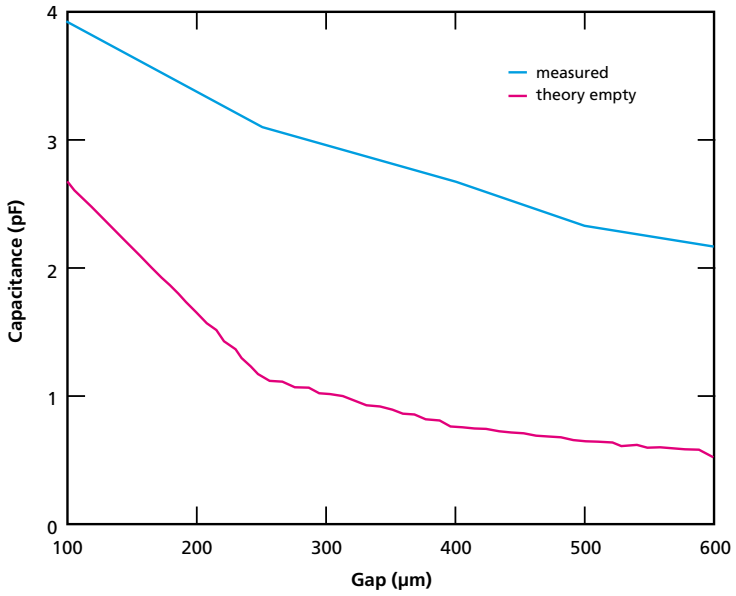

Measured and theoretical empty LAC capacitance against gap size.

The damage in this specific area may be due to the transmission line reflection of the lightning pulse at the PTFE end of the web as the damage spreads to the surface beneath the PTFE disk. Figure 6 has been extracted from technical drawings of the connector. It shows the chamfer of the web and the dimensions of the air gap with an indication of the 150 μm trigger particles to show that there will be particles within the chamfer area. The packing of the particles can only be assumed to be random as they are of random shape and the filling procedure was not consistent.

It may be possible to increase the air gap between the web and pin and add a protuberance to the web. This would ensure that the location of the breakdown occurred in the same area. Any protuberance would be greater in size than any single particle so there would be no problem with the arrangement of the particles

FIGURE 5

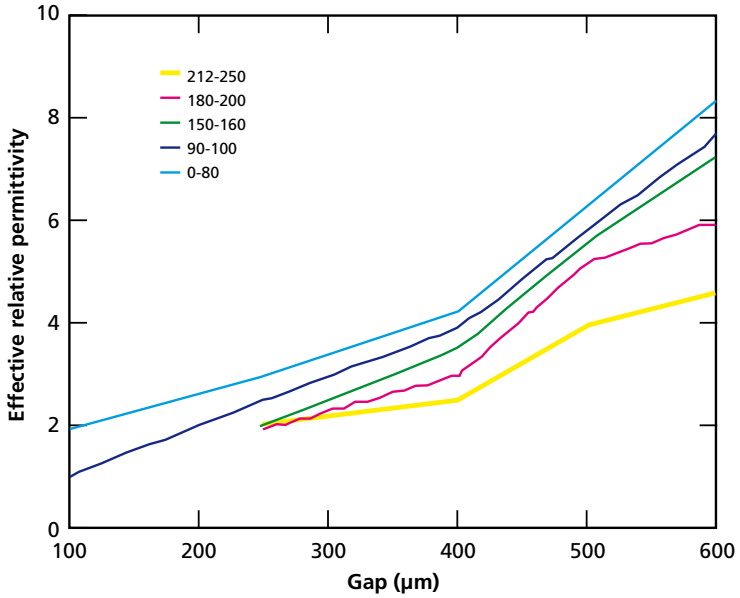

Effective relative permittivity of the loaded LAC for different particle size distributions.

"The lightning-arrester connector employs non-spherical trigger particles within a cavity between the pin and outer conductor of a coaxial cable geometry transmission line within the connector. "

with respect to the protuberance itself. The nature of the protuberance may cause problems when it comes to filling the air gap with the trigger particles and large voids occurring below the protuberance.

To aid in the understanding of the LAC the physical and electrical properties of the LAC were modelled. The rutile particles used in LACs are not spherical, as can be seen in the SEM micrograph in Figure 7. Box 1 provides some information on non-uniform packaging which was used during the modelling of the rutile material. The rutile particles were approximated as two spheres of varying permittivity, as shown in Figure 8.

The two spheres were arranged such that the inner sphere is the largest sphere that is fully contained within the particle and thus had a ε_r of 100. Using a simplification of Bruggeman's formula, the relationship between permittivities can be expressed as:

$$2 \quad \frac{\varepsilon_{eff} - \varepsilon_e}{\varepsilon_{eff} + 2\,\varepsilon_e} = f_1 \frac{\varepsilon_1 - \varepsilon_e}{\varepsilon_1 + 2\,\varepsilon_e} + f_2 \frac{\varepsilon_2 - \varepsilon_e}{\varepsilon_2 + 2\,\varepsilon_e}$$

$$\varepsilon_1 = 61\varepsilon_e \quad \varepsilon_2 = 100\varepsilon_e \quad f = f_1 + f_2 = 0.3 \quad \varepsilon_e = \varepsilon_o$$

FIGURE 6

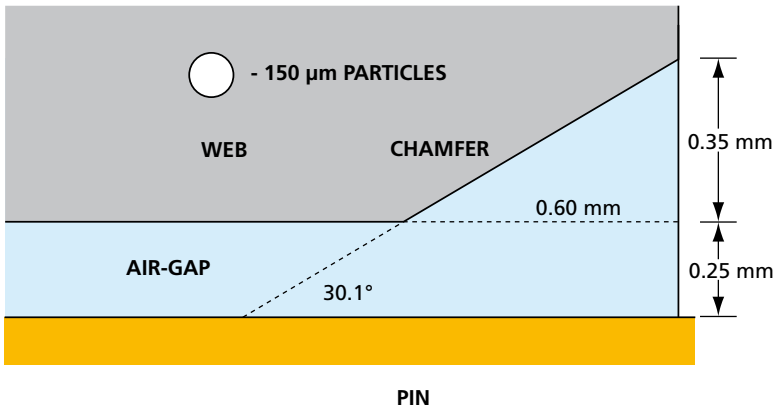

Chamfer geometry.

The outer sphere is a sphere that fully contains the particle and so will contain air. The permittivity of the outer sphere requires a volume factor that is not constant for the infinitely different shapes that can be formed. Using the results obtained from capacitance measurements and simulations a factor of 0.3 was used, resulting in an ε_{eff} of approximately 5.

The permittivity of the rutile particle can be used in the calculation for breakdown of the material. The classical Townsend theory of the breakdown in dielectrics gives the steady state condition for a uniform applied electric field and is given by Auer[9] as

$$3 \quad \frac{\beta}{\alpha}\left[e^{\alpha\delta} - 1\right] = 1$$

Where α is the primary ionisation coefficient β is the secondary ionisation coefficient for photoelectric production at the cathode and δ is the separation of the anode and cathode. Although this is derived for the steady state condition Auer has shown that the same condition applies for the transient condition. For a non-uniform electric field ($\boldsymbol{E}$) the condition given in equation 3 can be generalised to

$$4 \quad \beta \int_{x_0}^{x_1} e^{\alpha E x}\, dx = 1$$

Where x is the position along an electric field line from x_0 to x_1. Using the parameters given by Miyoshi[10] the dielectric breakdown for the empty LAC can be calculated using equation 4. Figure 9 shows a comparison of

FIGURE 7

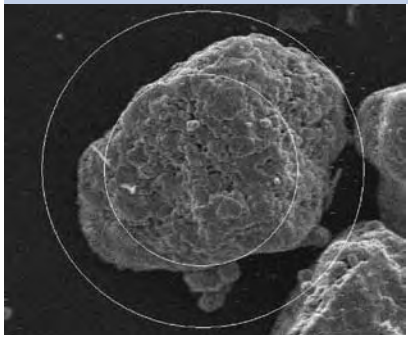

Representative micrograph of rutile particle shapes.

FIGURE 8

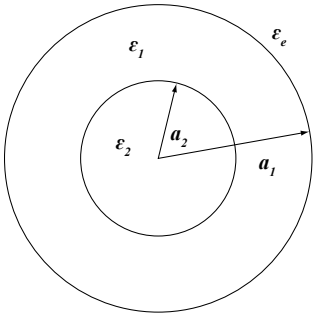

Different permittivity, irregular shaped particles modelled as layered spheres.

FIGURE 9

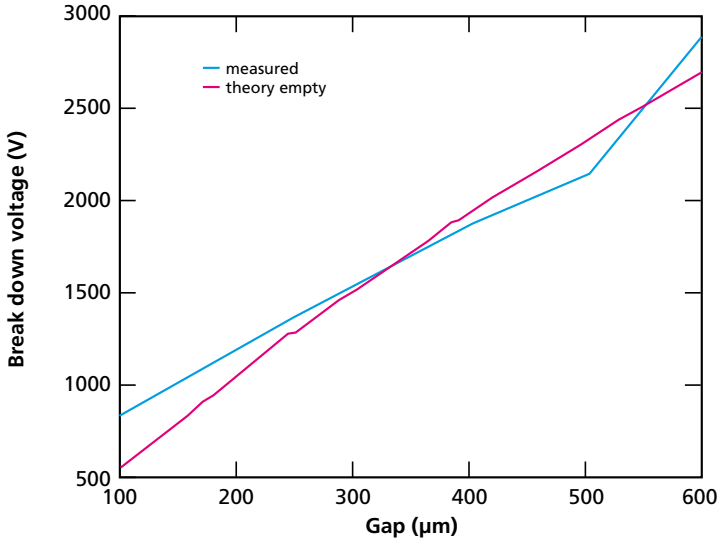

Breakdown voltage of the empty LAC compared with the theoretical Townsend breakdown voltage.

FIGURE 10

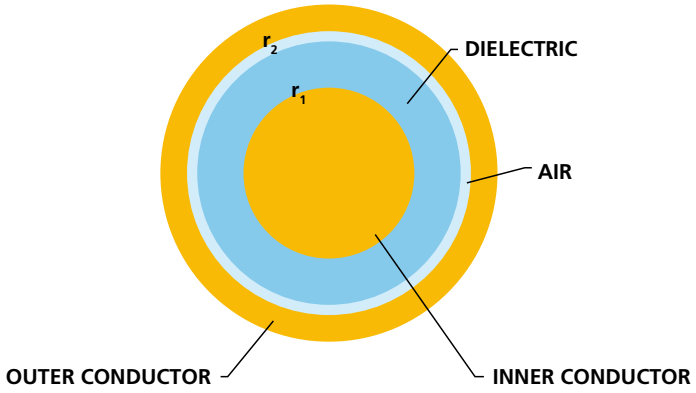

Approximate geometry for estimating the breakdown voltages in the voids of the loaded LAC.

calculated breakdown voltages with measured voltages for varying gap sizes.

Assuming that the effective relative permittivity of the loaded LAC is about 5 and the air gaps are approximately half the diameter of the particles then the breakdown of the air gaps or voids in the loaded LAC can be estimated using the geometry given in Figure 10.

The radial distance (r_2-r_1) is taken to be the void diameter or half the particle diameters and the solid dielectric permittivity is the effective permittivity of the bulk particles ($\varepsilon_r = 5$) . Using the very approximate geometry with the parameters given by Miyoshi and equation 4 the dielectric breakdown for different particle sizes and LAC sizes is as given in Figure 11.

Conclusions

The lightning-arrester connector employs non-spherical trigger particles within a cavity between the pin and outer conductor of a coaxial cable geometry transmission line within the connector. The calculated results shown in Figure 11 show broad agreement with the measurements in Figure 2. This indicates that the LAC breakdown is triggered by the air breakdown in a void in the particle dielectric. The arc may then develop from either the resulting photon emissions triggering other voids to breakdown or the other voids may breakdown as a result of the

FIGURE 11

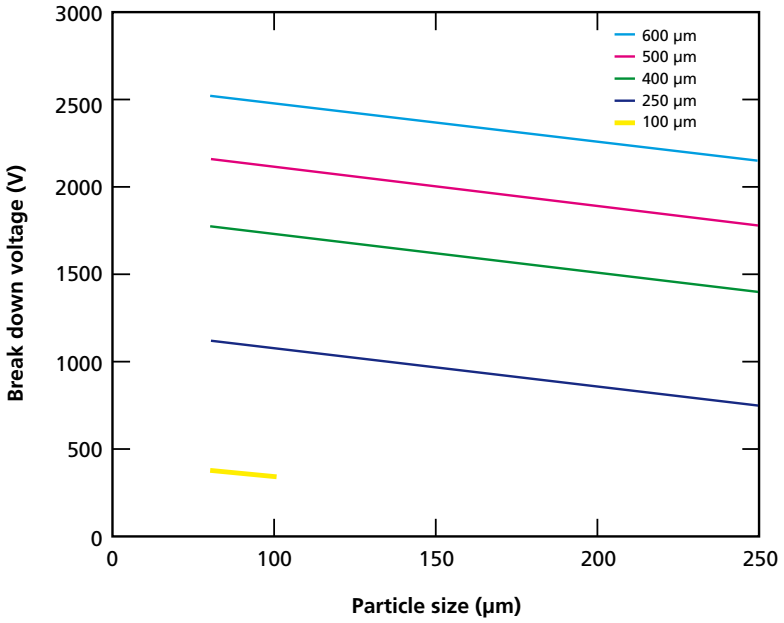

Estimated breakdown voltage for the air voids in loaded LACs against particle sizes and for different LAC dimensions.

sudden increase in electric field strength resulting from the initial discharge. The semiconductor properties of the rutile may also play a part in the subsequent arc development. Further work is in progress to refine the models of the rutile particles and to increase understanding of trigger materials.

Acknowledgements

The author would like to thank the contributions of Dr R Lynch, L Clark and S Hellston throughout the work characterising the connectors and also with the preparation of this article.

References

1 M. Brook, C. R. Holmes, and C. B. Moore, "Lightning and Rockets: Some implications of the Apollo 12 lightning event," Naval Research Reviews, pp. 1 - 17, 1970.

2 Franz Fuchs, Ernst Ulrich Landers, Rudolf Schmid, and Johannes Wiesinger, "Lightning Current and Magnetic Field Parameters Caused by Lightning Strikes to Tall Structures Relating to Interference of Electronic Systems," IEEE Transactions on Electromagnetic Compatibility, vol. EMC-40, pp. 444 - 451, 1998.

3 J Arlin Cooper and L. J. Allen, "The Lightning Arrestor-connector Concept: Description and Data," IEEE Transactions on Electromagnetic Compatibility, vol. EMC-15, pp. 104 - 110, 1973.

4 Richard K Traeger and Edward F Ehrman, "The Lightning Arrestor Connector," IEEE Transactions on Parts, Hybrids and Packaging, vol. PHP-12, pp. 89 - 94, 1976.

5 John P. Brainard and L. A. Andrews, "Dielectric Stimulated Arcs in Lightning-Arrestor Connectors," IEEE Transactions on Components, Hybrids, and Manufacturing Technology, vol. CHMT-2, pp. 309 - 316, 1979.

6 ANSI, "Standard Test Method for Dielectric Breakdown Voltage and Dielectric Strength of Solid Electrical Insulating Materials Using Impulse Waves," ASTM international, pp. 1 - 4, 2004.

7 J M Meek and J D Craggs, "Electrical breakdown of gases", Pub. Clarendon Press, Oxford 1953, ISBN 0 471 995533

8 H Lau, "Landolt-Bornstein: Zahlenwerte und Funktionen aus Physik, Chemie Asteonomie, Geophysik und Technik, Vol. 4, Part 3, p105, Pub. Springer-Verlag, Berlin, 1957.

9 P. L. Auer "Phenomenological theory of Townsend breakdown in dielectrics" Physical Review, Vol. 98, No. 2, April 15, 1955, pp 320-327.

10 Yasunori Miyoshi "Theoretical analysis of build-up of current in transient Townsend discharge" Physical Review, Vol. 103, No 6, Sept. 15, 1956 pp 1609-1618.Box 1

11 G.G. Szpiro (2003) Kepler's Conjecture Wiley, John & Sons Inc. ISBN 0-471-08601-0

12 T. Aste and D. Weaire "The Pursuit of Perfect Packing" (Institute Of Physics Publishing London 2000) ISBN 0-7503-0648-3

BOX 1

Kepler's Conjecture

The face-centred (hexagonal) cubic packing of spheres of the same radius in three dimensions has the greatest density (similar to cannonball stacking). This was first claimed by Johannes Kepler in his paper "The Six-Cornered Snowflake"[11] a paper inspired by his communication with Thomas Harriot. In his essay, Kepler stated that face-centred cubic packing, the kind the military used to stack cannonballs, is "the tightest possible, so that in no other arrangement could more pellets be stuffed into the same container."

In the nineteenth century, Carl Gauss proved that face-centred cubic packing is the densest arrangement in which the centres of the spheres form a regular lattice, but he left open the question of whether an irregular stacking of spheres might be still denser.

In 1953, László Tóth reduced the Kepler conjecture to a very large calculation that involved specific cases, and later suggested that computers might be helpful for solving the problem. This was the approach taken by Thomas Hales, a mathematician at the University of Michigan at Ann Arbor, and which led him, in 1998, to claim that he had proved Kepler was right after all.

Hales proof of Kepler's conjecture remains controversial simply because of the length of the calculations involved and the difficulty of verifying them.[12] Note that for spheres, according to Kepler's conjecture, the maximum volume fraction is:-

$$\frac{\pi}{3\sqrt{2}} \approx 74.048\%$$

and is independent of sphere size. Hence, the maximum expected relative effective permittivity from the rutile having an ε_r of 100 is $\varepsilon_{eff} = 61.77$.

AUTHOR PROFILE

Philip Shepherd can be contacted on e-mail: philip.shepherd@awe.co.uk

Philip Shepherd • Philip joined AWE in May of 2008 after completing a Post Doctorate at Nottingham University on the operation of the Lightning Arrester Connector contracted by AWE. His PhD was gained from the University of Warwick in 2006. Before that Philip worked at Filtronic Components Ltd in Bradford and prior to that the Defence Evaluation and Research Agency (DERA) in Portsmouth. He gained his Masters and Bachelors degrees at the University of Leeds in Electrical and Electronic Engineering. Philip now works in the Fire Unit team within AWE's Technology Division.

AWE's Outreach, Major Events and Collaborative Activities

2009 was another successful year of events, conferences and exhibitions for AWE. This article summarises a few key events in which AWE participated.

Top Set

The winners of the AWE Science, Engineering & Technology (SET) Awards 2008, were presented with their awards by guest of honour, Professor Mark Welland, chief scientific adviser to the Ministry Of Defence. Robin McGill, AWE chief executive officer, said:

"This is my first awards ceremony and I can clearly see why it is an important occasion for AWE and as such I pay tribute to the outstanding achievements of our superb award winners."

The Clive Marsh Award for innovative contribution demonstrating creativity at early career stage, was awarded to Dr. David Johnson.

The two JC (Charlie) Martin Awards recognise technical content, originality and presentation in an internal report or externally published paper. The Best External Paper was awarded to Mike Hutchinson for 'The escape of blast from fragmenting munitions casings', published in the International Journal of Impact Engineering. The Best Internal Report went to Alan Mears for his report 'Further analysis of KRAKATAU region 1'. Krakatau was an important experiment, performed in 2006.

The Chief Scientific Adviser Ministry of Defence Award, for pioneering breakthrough or discovery in the SET field, was presented to Chris Marsh. Chris developed an ingenious strong-link concept based on explicitly driven code events in a maze based arrangement to discriminate the unique signal. This innovation offers enhanced safety properties.

The John Challens Medal, which recognises sustained, high quality and valued contribution to the work of AWE in the SET field, was awarded to John Maw. John joined AWE over 40 years ago and made his principle contributions in the field of material modelling which led the development of AWE's online equation of state library. This area represents an essential component in Comprehensive Test Ban Treaty methodology. Professor Welland said:

"The winners are inspirational exemplars for the UK's science and engineering industry and have much of which to be proud."

SET AWARDS 2008 WINNERS

Standing from left to right: Chris Marsh, Chief Scientific Adviser Ministry Of Defence Award winner; John Maw, John Challens Medal winner; Alan Mears, JC (Charlie) Martin Award winner for Best Internal Report; Dr. David Johnson, Clive Marsh Award winner; Linda Hutchinson (wife of Mike Hutchinson, winner of JC (Charlie) Martin Award for Best External Paper); Ruth Chesseman (accepting award on behalf of Mike Hutchinson).

Sitting from left to right: Prof. Richard Clegg, former AWE chief scientist; Prof. Mark Welland, chief scientific adviser to the MOD; Robin McGill, AWE chief executive officer; Dr. Daryl Landeg, AWE chief scientist.

Shock Debate

The Institute of Shock Physics (ISP) awareness event was held on 15 May 2009 - over 100 staff and guests attended. Those who gave presentations included top academics Professor Steven Rose, director, ISP, Imperial College; Professor Paul McMillan,

ISP PRESENTERS

Professor Steven Rose speaking to delegates about recent appointments at Imperial College.

Left to right: Paul Hazell, Cranfield University; Prof. Paul McMillan, University College London; Don Cook, former AWE managing director; Peter Roberts, head, AWE Plasma Physics Department and Visiting Professor at Imperial College; Prof. Steven Rose, director, ISP, Imperial College.

University College London and Paul Hazell, Cranfield University.

This event was shaped by the AWE hosted Dynamic Compression of Condensed Matter conference (DCCM), held in December 2007, which was the catalyst to reinvigorating the UK's shock physics community leading to the launch, in March 2008, of the ISP at Imperial College, to which AWE is the only contributor.

AWE's crucial requirement, which underpins its investment in ISP, is to train and develop the next generation of staff in fundamental and experimental shock physics. Peter Roberts, head, AWE Plasma Physics Department and Visiting Professor at Imperial College, said:

"Our vision is to develop a robust AWE shock physics gateway to academia that can act as a training provider and research partner."

The event successfully aimed to raise the profile of ISP and its benefits, not just to AWE, but to the UK as a whole.

The teaching and research will enable the recruitment of new graduates, provide enhanced learning, permit access to different innovative research areas, build the generation of ideas, promote short courses and experimental secondments.

The Italian Job

On 6 – 10 September 2009 the Italian village of Sestri Levante played host to the 28th meeting of the Polymer Degradation Discussion Group (PDDG). The event was well supported by members of AWE's materials science community. The PDDG is a branch of The Royal Society of Chemistry Macro Group which aims to encourage open and unscripted discussion and to give younger researchers the opportunity to meet leading scientists.

The meeting discussed nanocomposites, multifunctional materials and coatings/foams in the environment. In addition, a number of oral and poster presentations were given by AWE delegates on a wide range of cutting-edge materials science research topics.

The event was well attended by Department of Energy staff, and delegates from UK academia who have links with AWE.

University of Bristol Strategic Alliance

In November 2009, AWE formed a Strategic Alliance with the University of Bristol. Bristol now joins Imperial College, Cambridge,

PDDG DELEGATES

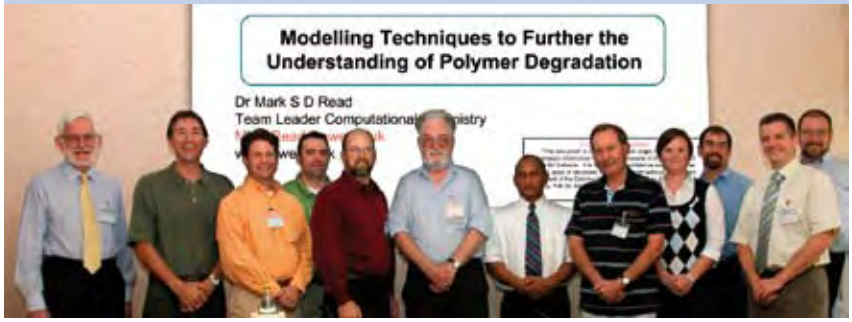

Left to right: Professor Dick Pethrick, University of Strathclyde; Dr. Mat Celina, Sandia National Lab; Dr. Dan Bowen, Kansas City Plant; Dr. Eric Eastwood, Kansas City Plant; Mr. LeRoy Whinnery, Sandia National Lab; Professor Norman Billingham, University of Sussex, editor in chief of Polymer Degradation and Stability Journal; Dr. Mogon Patel , AWE; Professor Graeme George, Queensland University; Mrs. Alison Hall, AWE; Dr. Robert Bernstein, Sandia National Lab; Dr. Mark Read, AWE; Dr. Robert Maxwell, Lawrence Livermore National Lab.

Cranfield and Heriot-Watt Universities. Chris Lord, AWE Technical Outreach strategy manager said:

"One of the key aims of this alliance is to maximise the impact and value of AWE's investments in knowledge and academia."

Professor Geoff Allen, former director Interface Analysis Centre, University of Bristol, has recently been appointed William Penney Fellow at AWE.

Condensed Matter and Materials Physics CMMP09

The CMMP group conference was held on 15 – 17 December 2009 at the University of Warwick. CMMP, an internationally recognised annual event for the UK's physics community, has provided a forum for researchers to present their work, either in symposia or in poster sessions. Over 350 physicists and scientists from a number of UK universities attended the conference, including delegates from AWE.

The event was co-sponsored by AWE, the Engineering and Physical Sciences Research Council, IOP Publishing and the University of Salford. The conference included a wide range of symposia, with speakers and contributions from the UK and abroad. The plenary invited and contributed presentations, along with poster sessions, covering the most exciting and topical aspects of condensed matter and material physics.

AWE owned the 'Matter under extreme conditions' symposium chaired by Dr. Andrew Gregory, AWE warhead safety adviser. Dr. Graham Ball, AWE group leader, Materials Modelling, Design Physics, led AWE's technical contribution.

Graham gave a presentation entitled: 'Challenges in modelling materials under extreme conditions', to postgraduate students expected to become the physicists of the future.

An exhibition was held alongside the conference to showcase AWE's work in materials modelling research, commitment to the Institute of Shock Physics, development of Strategic Alliances with UK universities and the Orion laser activity. The exhibition provided an ideal setting for UK wide researchers, scientists, developers, engineers and systems integrators with the opportunity to mix on a range of levels.

Other events supported during 2009 included the Dstl Internal Symposium, held on 17 - 18 June at the University of Surrey and the 4th Foam Workshop, held on the 2 - 3 September at AWE.

A number of prestigious events are scheduled for 2010 including the Nitrocellulose conference, the Condensed Matter and Materials Physics conference and the Plutonium Futures event.

If you are involved in an AWE technical event that you would like the editorial team to consider featuring in future editions of Discovery, please contact:

Paul Sagoo
Events & Communications Manager
Email: Paul.Sagoo@awe.co.uk

Discovery

Find out more about AWE at our website:

www.awe.co.uk

For further copies of this journal and details of other AWE publications, please write to:

Corporate Communications Office
Building F161.2
AWE Aldermaston
Reading
Berkshire
RG7 4PR

Printed on cocoon 100 silk

Please place FSC logo here

AWE is the trading name of AWE plc
Registered office: Aldermaston Reading Berkshire RG7 4PR
Registered number 3664571

The Science & Technology Journal of AWE • Issue 20 • May 2010